NASA TECHNICAL MEMORANDUM

NASA TM X-2475

NASA TM X-2475

THERMAL DESIGN STUDY OF AN AIR-COOLED PLUG-NOZZLE SYSTEM FOR A SUPERSONIC-CRUISE AIRCRAFT

by John S. Clark and Arthur Lieberman

Lewis Research Center

Cleveland, Ohio 44135

NATIONAL AERONAUTICS AND SPACE ADMINISTRATION • WASHINGTON, D. C. • JANUARY 1972

THERMAL DESIGN STUDY OF AN AIR-COOLED PLUG-NOZZLE SYSTEM FOR A SUPERSONIC-CRUISE AIRCRAFT

by John S. Clark and Arthur Lieberman

Lewis Research Center

SUMMARY

The cooling requirements of a plug-nozzle system for a supersonic-cruise aircraft engine have been studied. The engine selected provides a thrust of 267 000 newtons (60 000 lbf) and is designed for supersonic flight at speeds up to Mach 2.7. The plug is sting supported from the turbine frame. The conical plug selected has a 10° half angle and may be convection cooled on the sting support and plug up to the 50-percent point. The convection cooling air is then injected as a film over a conical plug extention that is truncated at the 75-percent point on the plug (i.e., 75 percent of the distance between the primary nozzle throat and the tip of the plug). The flight profile selected includes maximum afterburning from takeoff to Mach 2.7. A low afterburner setting is assumed for the supersonic-cruise portion of the flight.

The calculations indicate that, for maximum afterburning, about 2 percent of the engine primary air, removed after the second stage of a nine-stage compressor, should adequately cool the plug and sting support. During supersonic-cruise operation, ram air should adequately cool the plug. If about 1.5 percent ram air is used, the maximum plug wall temperature should be about 978 K (1760° R). If 0.5 percent ram air is used, the maximum plug wall temperature should be about 1133 K (2040° R).

INTRODUCTION

The cooling requirements have been studied for an air-cooled plug-nozzle system on a supersonic-cruise afterburning turbojet aircraft engine to determine the source of cooling air necessary to minimize the cycle penalty. The airplane chosen for this study was assumed to have a takeoff gross weight of 340 000 kilograms (750 000 lbm) and a payload of 6.5 percent of the takeoff weight. (The International System of Units will be used throughout this report as the primary system; U.S. Customary units will be included in

parentheses. Calculations were made using the U.S. Customary units). Each of four afterburning turbojet engines were assumed to provide a thrust of 267 000 newtons (60 000 lbf), and the cruise flight speed was assumed to be Mach 2.7.

In reference 1, the performance of a plug-nozzle system was compared with ejector nozzle systems. The optimum performance of a plug nozzle (assuming an uncooled plug) and of a variable-flap ejector was excellent and about equal. The performance of the auxiliary inlet ejector was slightly lower. However, the plug nozzle has certain advantages over the ejector nozzles:

(1) Leakage between moveable surfaces would be significantly lower since the length of seal required could be reduced from about 91.4 to 9.14 meters (300 to 30 ft).

(2) The mechanisms could be simpler and more durable.

(3) Jet noise tests indicate that the plug nozzle is a little quieter than the ejector nozzles (ref. 2).

Tending to offset these advantages, however, is the fact that the plug nozzle must be cooled during afterburning operation since it is immersed in the high-temperature primary jet. Reference 1 showed the effect of nozzle cooling on a typical supersonic-cruise mission for (1) a plug nozzle cooled with engine fuel and (2) an air-cooled plug nozzle using high-pressure compressor discharge air for the coolant. If engine fuel could be used to cool the plug, thus not reducing the engine cycle efficiency, the plug nozzle and variable-flap ejector would provide about the same range (about a 3 percent greater range than an auxiliary-inlet ejector). However, if compressor discharge air were used to cool the plug, the cycle efficiency would drop so that the plug showed little advantage in range over the auxiliary-inlet ejector. The purpose of this report is to show that cooling air for the plug may be removed from an earlier stage of the engine compressor without reducing the engine cycle efficiency as much. If this can be done, the plug-nozzle system will approach the same range as the variable-flap ejector.

There are, of course, several trade-offs involved in the design of a nozzle system. Among these are nozzle thrust performance, nozzle weight, noise, infrared radiation suppression, and some life criterion. Nozzle thrust performance and nozzle weight are functions of the type of nozzle and the nozzle-cooling requirements. For a nozzle cooled partially by film cooling, the location of the film-cooling slot affects nozzle performance, weight, and, of course, the nozzle-cooling requirements. Noise becomes important for commercial supersonic-cruise aircraft during flight over land and near airports. Infrared radiation suppression is desirable in certain military applications. Finally, nozzle life criterion may be different for commercial or military applications.

Since the plug-nozzle system is quieter than ejector nozzles and can be made to suppress infrared radiation (by overcooling, for example), a study of the plug cooling requirements and the resulting performance, weight, and life appears warranted.

The cooling technique used in this study is similar to the method used in reference 3. The plug in reference 3 was strut supported to the engine nacelle. A sting-supported

plug was selected for this study to eliminate the struts that were immersed in the hottest region of the hot gas. The cooling technique combines parallel-flow convection cooling and film cooling. The convection-cooling technique was studied in reference 3; thrust performance of an uncooled version of the plug used in reference 3 was presented in reference 4. Jeracki (ref. 5) studied the effect of discharging the convection cooling air as a film on a plug extension. Finally, Chenoweth (ref. 6) has studied the heat-transfer characteristics of a film-cooled plug. Each of these reports has been drawn upon in this report in an attempt to optimize the design.

This report studies the cooling requirements of only the plug and sting support. It is assumed that the cooling requirements of the secondary shroud, iris primary, and afterburner liner are about the same as an ejector nozzle.

SUPERSONIC-CRUISE AIRCRAFT FLIGHT REGIME

The flight profile selected for this study is shown in figure 1 and is assumed to be typical of a commercial supersonic-cruise mission. Figure 1(a) presents altitude, and

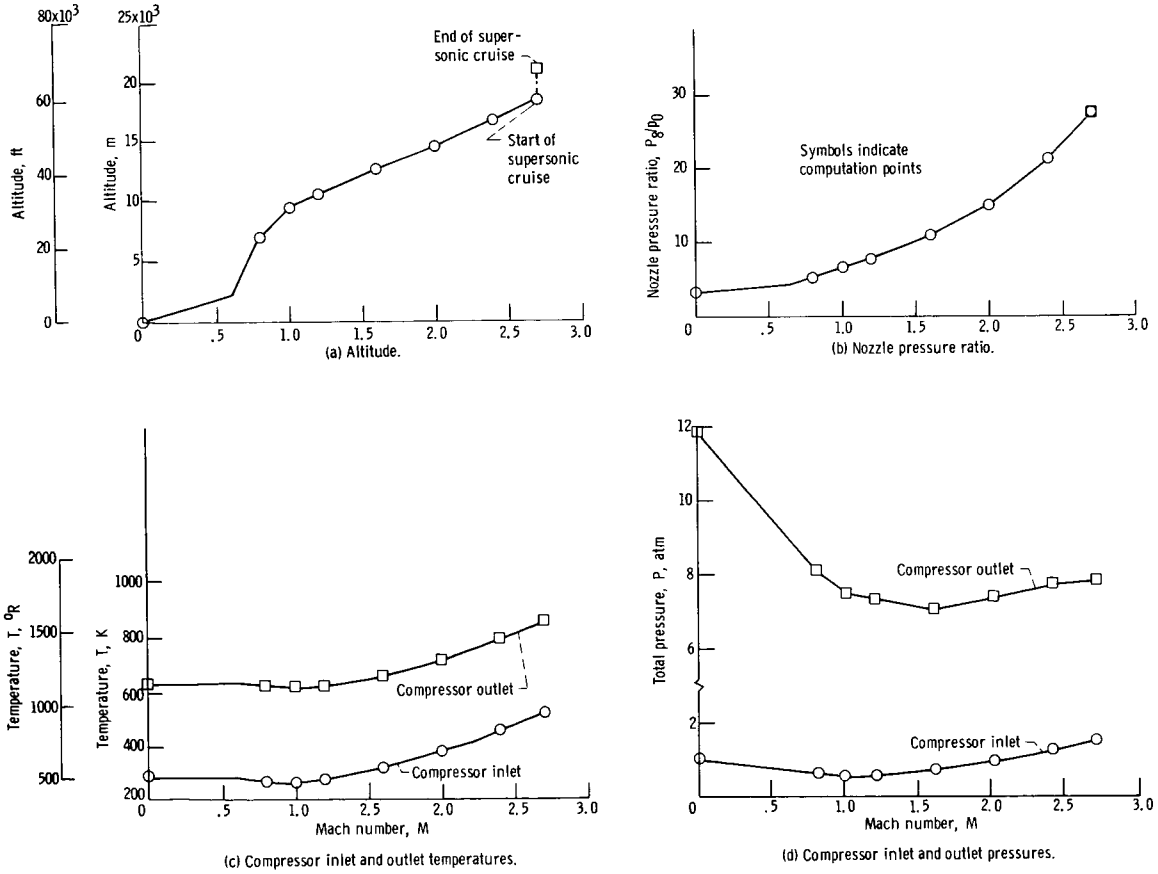

Figure 1. - Supersonic cruise aircraft flight profile.

TABLE I. - NOZZLE OPERATING CONDITIONS

Mach number, M	Altitude		Primary flow rate, $\dot{w}$		Nozzle total pressure, P_8, atm	Nozzle total temperature		Ambient pressure, p_0, atm	Nozzle pressure ratio, p_8/p_0
	m	ft	kg/sec	lbm/sec		K	^{o}R		
0	0	0	287	633	3.03	1945	3500	1.0	3.03
.8	7 010	23 000	189	416	2.10	1945	3500	.405	5.18
1.0	9 450	31 000	172	378	1.83	1945	3500	.284	6.46
1.2	10 500	34 500	170	375	1.87	1945	3500	.241	7.75
1.6	12 650	41 500	166	365	1.89	1945	3500	.173	10.88
2.0	14 500	47 500	173	381	1.94	1945	3500	.129	14.99
2.4	16 600	54 500	182	401	1.97	1945	3500	.093	21.28
[a]2.7	18 300	60 000	186	410	1.97	1945	3500	.071	27.6
[b]2.7	18 300 - 20 750	60 000 - 68 050	186	410	1.97 - 1.35	1347 - 1286	2425 - 2314	0.071 - 0.049	27.6

[a]End of acceleration.

[b]Start (first value) and end of supersonic cruise.

figure 1(b) shows nozzle pressure ratio, both as functions of Mach number, during the acceleration portion of the assumed flight. A Brequet cruise was also assumed; the altitude of the aircraft increases from 18 300 to 20 750 meters (60 000 to 68 050 ft) as the fuel is burned. Table I presents nozzle operating conditions used in this study. (Symbols are defined in appendix A). Maximum afterburning is assumed during acceleration up to Mach 2.7; the afterburner is assumed to be on at a low setting during supersonic cruise. The compressor is assumed to have nine stages. Figures 1(c) and (d) show the compressor-inlet and compressor-outlet total temperature and total pressure, respectively, as functions of Mach number.

NOZZLE CONFIGURATION

The afterburner-nozzle configuration is shown schematically in figure 2. The 10^{o} plug is sting mounted to the turbine frame. The outer afterburner wall is shielded from the afterburner flame with a perforated liner. Turbine discharge air is forced between the wall and the liner and film cools the liner. An iris primary nozzle was selected to provide variable primary area for the various engine conditions. The iris primary is film cooled with the remaining turbine discharge air at the end of the afterburner liner.

A translating, cylindrical secondary shroud was assumed to vary the hot-gas expansion ratio and maintain efficient nozzle performance over the required range of nozzle pressure ratios. Reference 7 showed that little loss in performance resulted by using a two-position shroud. A retracted shroud could be used for takeoff and acceleration up to Mach 1.2; then the shroud could be fully extended for speeds up to and including Mach 2.7. For the nozzle selected for this study, the retracted position is the -14.4-percent

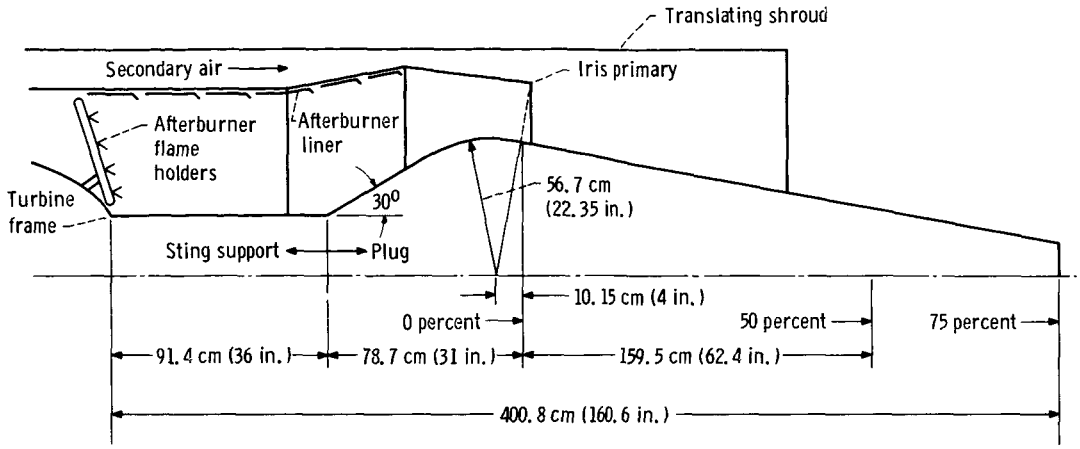

Figure 2. - Plug nozzle centerbody configuration.

point (upstream of the primary throat), and the extended position is the 38-percent point (see fig. 3).

The 75-percent truncation point was selected to reduce the overall length of the nozzle; reference 4 indicates that this truncation should not affect the thrust at high pressure ratios but would decrease the thrust coefficient about 1/2 percent at takeoff.

Figure 3 shows the detailed geometry assumed for this study. The dimensions shown for the primary nozzle are for the maximum afterburning position. For nonafterburning or low afterburning, the primary nozzle area must be decreased.

The proposed sting and plug may be convectively cooled to the 50-percent point along the plug surface as shown in figure 3, that is, half-way between the primary throat and the end of a full cone. The conical extension between the 50-percent point and the 75-percent point then could be film cooled with the air discharging from the convective-

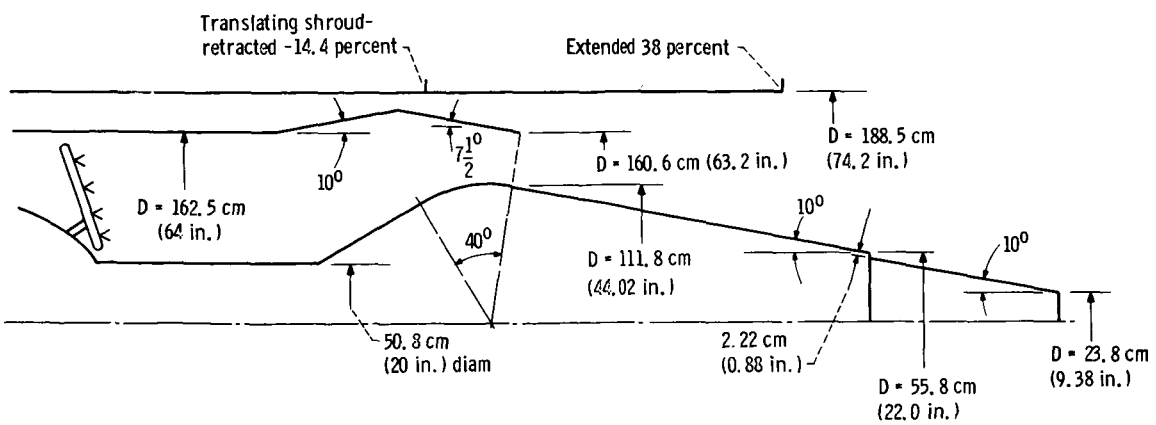

Figure 3. - Plug nozzle geometry (maximum afterburning). Convection cooling to 50 percent, film-cooling to 75 percent.

cooling passages. The trade-offs involved in selecting the optimum point to begin film cooling will be discussed in a later section of this report.

Details of the convective-cooling passages in the plug and sting support are shown in figures 4 and 5. This method was used successfully on an air-cooled plug in a J-85-GE-13 engine (ref. 3). The plug used in the experimental study of reference 3 was 40.6 centimeters (16 in.) at its maximum diameter and was convectively cooled to the 60-percent truncation point. The plug of reference 3 was strut supported. The fabrication technique involved brazing nickel fins onto the inside surface of the high strength plug wall. The cooling channel was completed by attaching a thin inner wall. The plug was built in axial sections. An expansion seal was incorporated between each section at the

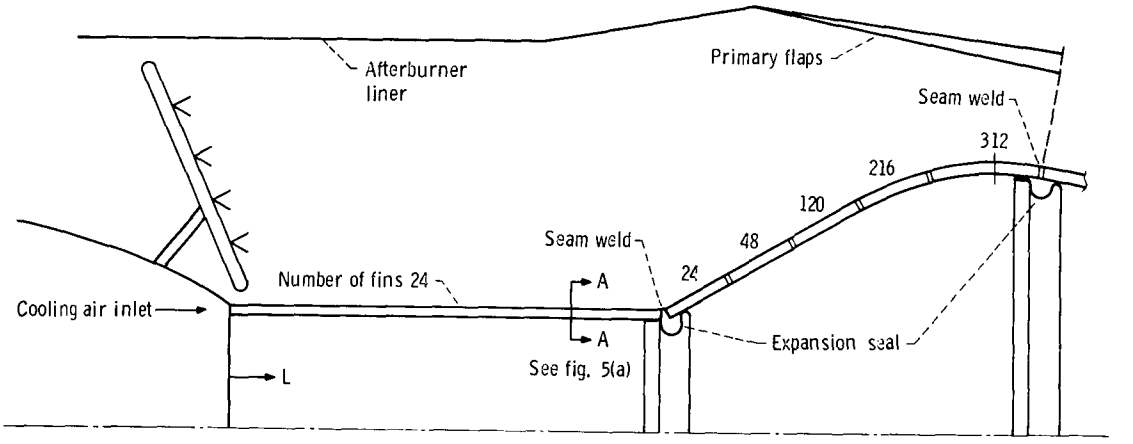

(a) Subsonic region.

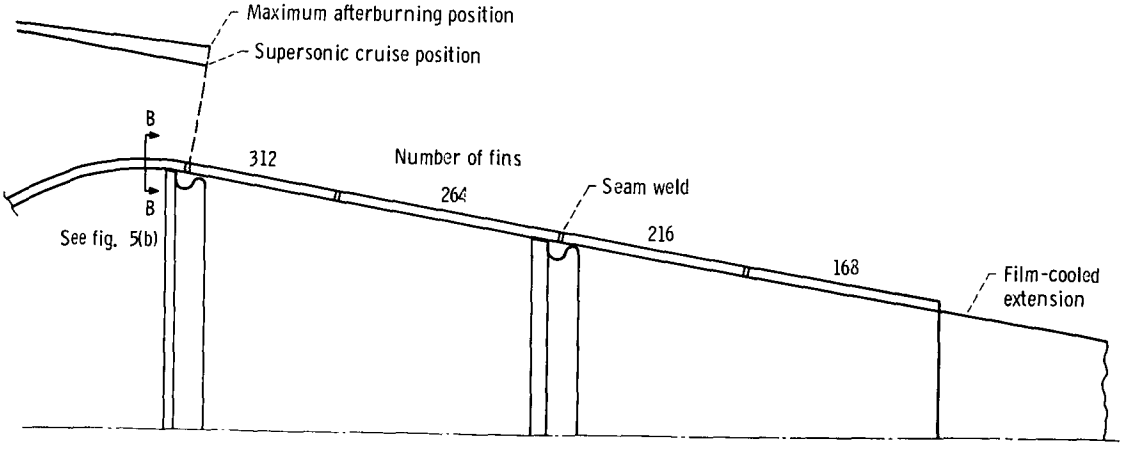

(b) Supersonic region.

Figure 4. - Convection cooling passages.

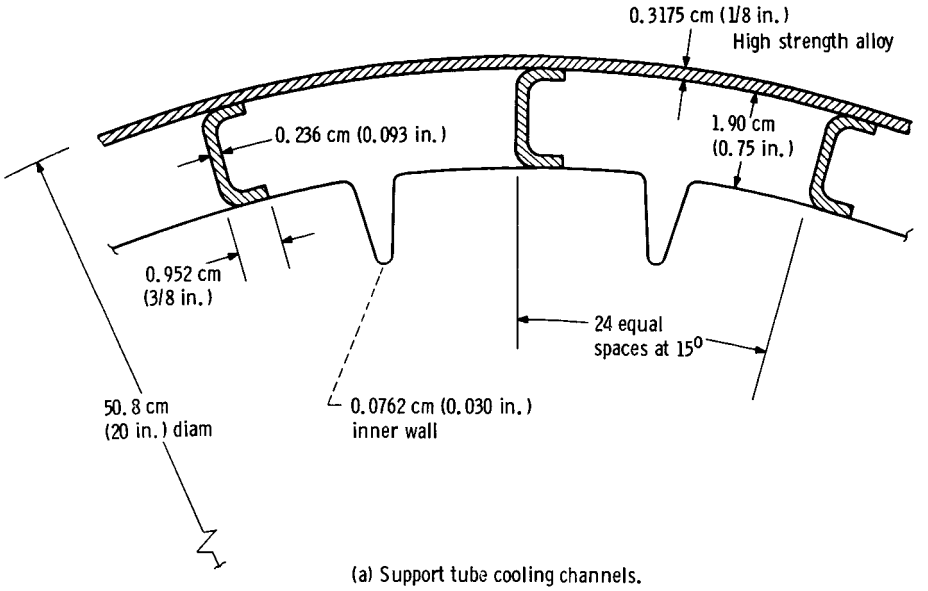

(a) Support tube cooling channels.

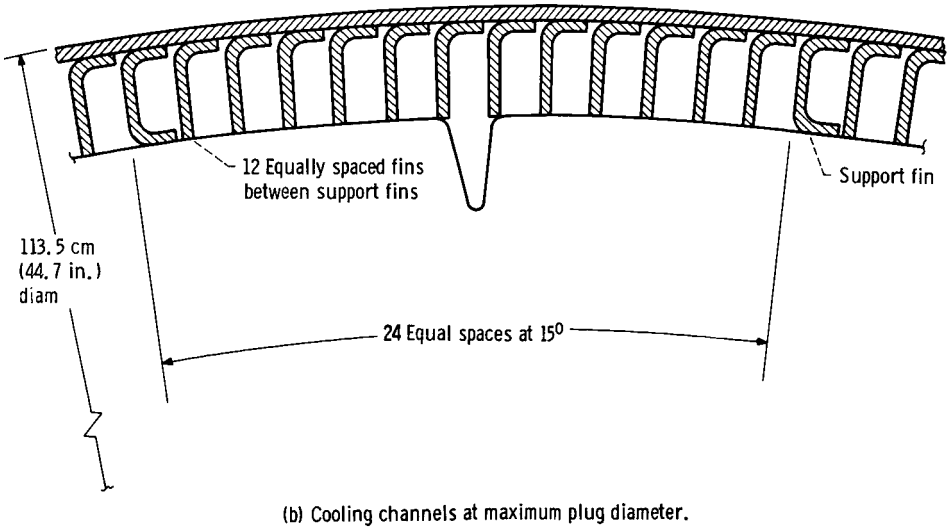

(b) Cooling channels at maximum plug diameter.

Figure 5. - Cooling channel configuration.

inner wall, and the outer wall of each section was seam welded to complete the plug. The expansion seals are required to allow thermal expansion of the hot outer wall relative to the cooler inner wall.

The fin geometry selected for this study was scaled up by a factor of three from the plug used in reference 3; the outer wall was only doubled, however. A preliminary stress analysis of this wall is discussed in the section OTHER CONSIDERATIONS.

The spacing of the nickel fins, and hence the number of fins around the circumference of the plug (fig. 4), was chosen to yield approximately uniform plug wall temperatures. Uniform high wall temperatures would result in the lowest heat transfer from the hot gas to the wall, and, hence, require the least cooling air. Figure 5(a) shows a cross section through the support tube, and figure 5(b) shows a section at the maximum plug diameter. The dimensions shown for wall thickness, fin thickness, and fin height are assumed to be the same for the plug and sting support. Fins are shown in the support tube spaced at 15^{o} increments. The fins in the support tube are included to maintain uniform coolant-passage heights in the support tube and to increase the rigidity of the support tube. More fins may be added in the support tube, if desired, to lower the wall temperatures and increase the strength of the sting support.

In each section of the plug assembly, the inner wall will be attached to the C-shaped fins on the downstream end of that section only. The L-shaped fins are not attached to the inner wall. The plug inner cavity should be maintained at the coolant-inlet pressure, thus insuring that the inner wall will be pressed against the fins.

HEAT-TRANSFER DESIGN PROCEDURE

Convective Cooling

The procedure used to design the convectively cooled plug reported in reference 3 was also used in this study. Briefly, beginning with known hot-gas conditions, geometry, and coolant-inlet conditions, a heat balance is performed at many stations along the surface of the plug (see fig. 6(a)). Convective heat transfer from the hot gas to the plug wall is included, as is radiation from the hot flame to the wall. Radiation interchange between the plug and the afterburner liner, primary nozzle flaps, secondary shroud, and atmosphere were neglected. High-speed flow effects were included. Pressure calculations were performed from the end of the convection-cooling passage upstream to the inlet to the sting support. Momentum and friction pressure drop were included. The effects of these assumptions and equations used are discussed in detail in appendix B.

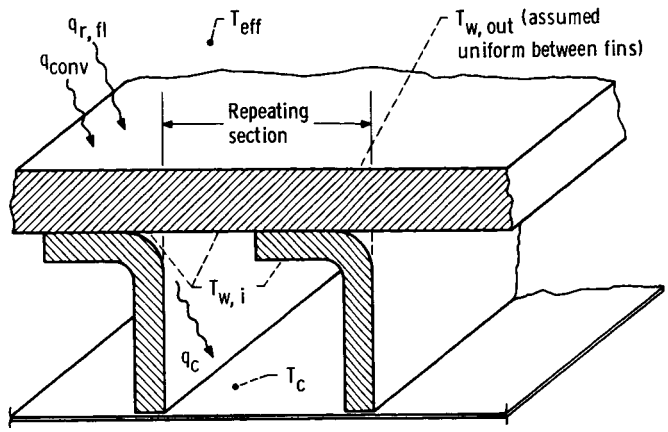

(a) Convection ($q_c = q_{conv} + q_{r, fl}$ and $q = 0$ at end of fin).

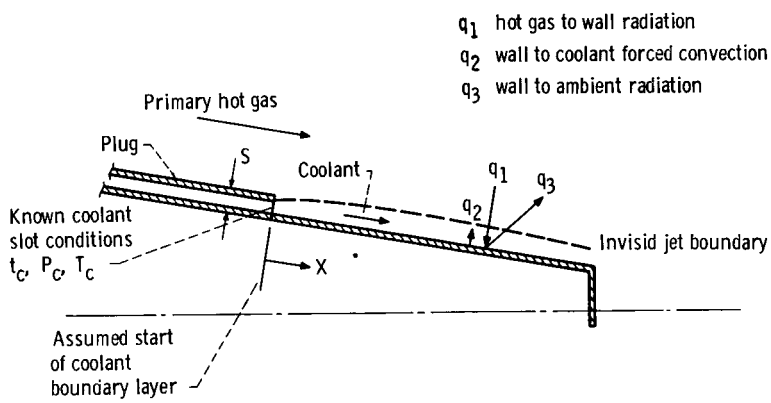

(b) Film cooling ($q_1 = q_2 + q_3$).

Figure 6. - Heat-transfer model.

Film Cooling

The film-cooling design procedure used to predict wall temperatures on the film-cooled extension used a modification of the method presented in reference 8, which predicted temperatures on a cylindrical ejector. Reference 8 used a wall heat balance which included hot-gas-to-wall radiation, convective heat transfer between the coolant stream and the wall, internal wall radiation from the ejector exit, external wall-to-ambient radiation, and external free convection. The plug wall heat balance used herein includes only hot-gas-to-wall radiation, convective heat transfer between the coolant stream and

the wall, and external radiation (see fig. 6(b)).

Flow fields were determined by assuming that the hot-gas jet and the coolant expanded isentropically along the plug and that the static pressure was uniform across the nozzle cross section. The film coolant was assumed to flow between the plug and the hot gas. Coolant stream properties beyond the slot were determined by assuming that the coolant stream had a recovery temperature equal to the adiabatic wall temperature as predicted by the Hatch-Papell (ref. 9) semi-empirical film-cooling correlation, thus accounting for thermal mixing of the hot-gas and coolant stream. The state of the coolant at the slot was assumed to be the state of the fluid at the end of the convective-cooling passages. The effect of the fins in the slot on the film-cooling effectiveness was neglected.

The technique for predicting the adiabatic (insulated) wall temperature on a plug nozzle was presented in reference 6 where it was compared with relatively low-temperature data. Reference 6 showed that, at takeoff and supersonic-cruise nozzle pressure ratios, the correlation provides good agreement between predicted and measured wall temperatures.

The method used to predict plug extension surface temperatures is discussed in detail in appendix C.

RESULTS AND DISCUSSION

Several flight conditions were analyzed in this study. Table I presents the nozzle operating conditions assumed for this study. The maximum-afterburning, sea-level-takeoff engine condition is critical since, at this condition, no ram air is available for cooling the plug. Therefore, the plug cooling air must be obtained from the compressor. On the other hand, at the supersonic-cruise flight condition with low afterburning, ram air is available and could be used with very little penalty to the cycle efficiency. The sea-level-takeoff and supersonic-cruise conditions are examined in detail, and a brief look is taken at some of the intermediate maximum-acceleration conditions: Mach 0.8, 1.0, 1.2, 1.6, 2.0, 2.4, and 2.7.

Sea-Level Takeoff

For sea-level takeoff with maximum afterburning, the nozzle total temperature was 1945 K (3500° R), the total pressure was 3.03 atmospheres (44.5 psia), the primary flow rate was 287 kilograms per second (633 lbm/sec), and the nozzle pressure ratio P_8/p_0 was 3.03.

Hot-gas pressure distribution. - To calculate local velocity and subsequently the local heat flux, the plug surface pressure distribution is required. The pressure distribution on a 10^{o} half-angle plug, operating at a nozzle pressure ratio of about 3.0, is characterized by a series of over-expansions and recompressions along the plug surface. Figure 7 shows experimental pressures from three separate experimental studies. The Chenoweth data (ref. 6) were obtained on a model with a 12.24-centimeter (4.82-in.) plug diameter and a full 100-percent plug in a static test facility. The maximum gas total temperature in the study was 555 K (1460^{o} R), and, for the data shown, a film-cooling slot was located at the 10-percent point on the plug. Reference 6 also showed that the position of the coolant slot did not significantly affect the plug pressure distribution. There was no secondary air used during the study. The Huntley data (ref. 4) were obtained on an uncooled plug installed on a turbojet engine. The plug model was 43.9 centimeters (17.3 in.) in diameter, and, for the data shown, had a corrected secondary weight flow ratio of 0.071. The engine was run at rated speed with no afterburning, which resulted in primary-gas total temperature of 922 K (1660^{o} R). The Bresnahan data (ref. 7) were also obtained on a 12.24-centimeter (4.82-in.) plug diameter model in both a static test facility and in a wind tunnel. Room-temperature air was used for both primary and secondary streams; there was no secondary flow for the data shown.

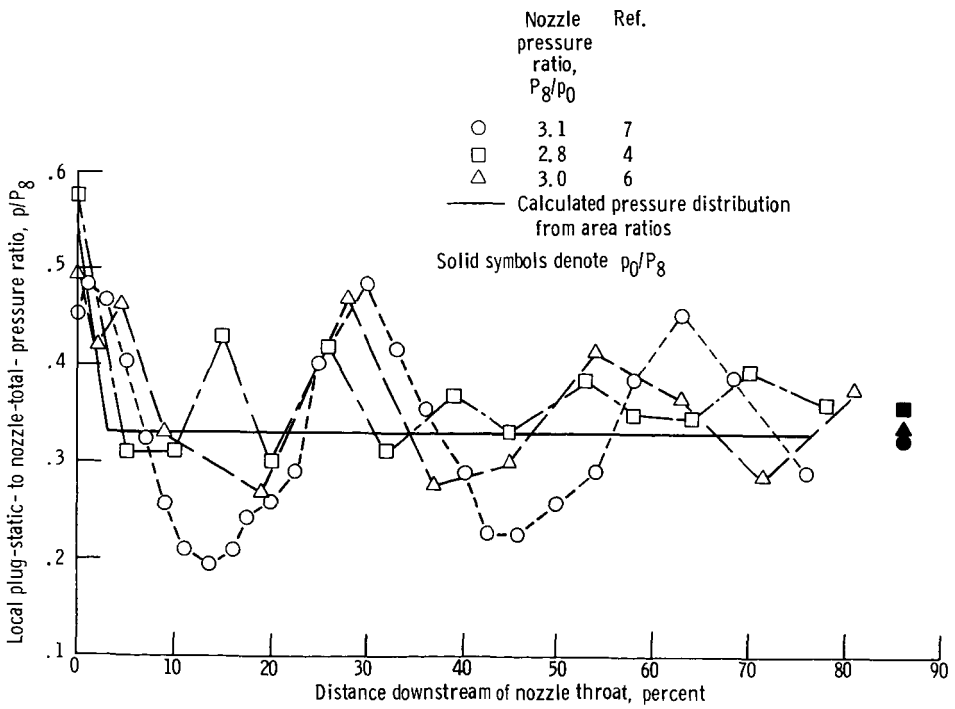

Figure 7. - Comparison of predicted and experimental pressures on plug surface. Sea-level takeoff, Mach 0.

The data shown in figure 7 indicate that the plug static pressure distribution is a strong function of nozzle pressure ratio; this is also shown in the other data of references 4, 6, and 7. No general method has been found in the literature to calculate these pressure distributions. The pressure distribution is a function of the total temperatures of the primary stream and the secondary stream and a function of the total pressures of the two streams. The geometry, especially at the sonic point, is also critical. Finally, a mixing model must be assumed between the primary and secondary stream and between the secondary stream and the atmosphere in order to calculate the pressure profiles. No attempt was made in this study to solve this complex problem. The solid line in figure 7 indicates the assumed pressure distribution used for this study. It was determined by the area-ratio method described in appendix B. A study was made of the effect of this assumption on the resulting wall temperatures and is discussed in the next section.

Comparison of heat-transfer coefficients. - Heat-transfer coefficients must be known to calculate wall temperatures. Figure 8 shows a comparison of several methods of cal-

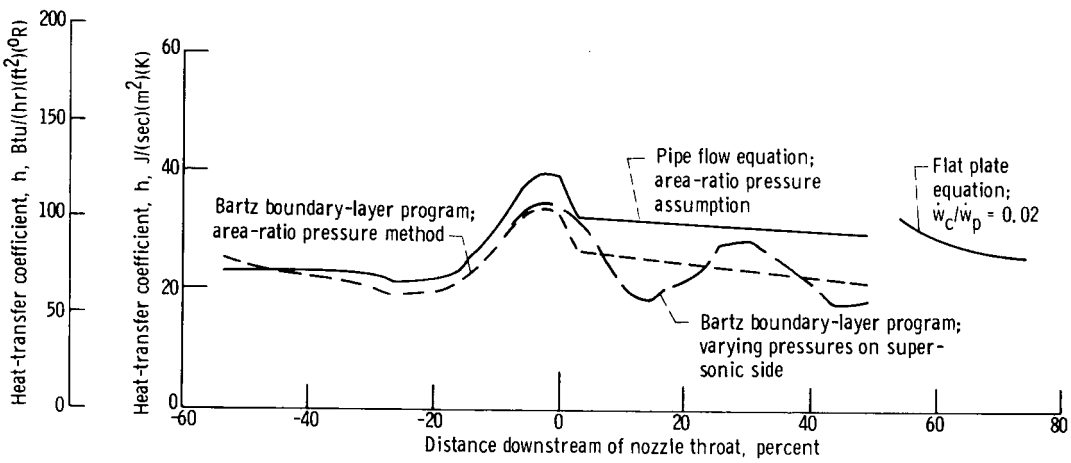

Figure 8. - Comparison of convective heat-transfer coefficients for sea-level takeoff and maximum afterburning.

culating heat-transfer coefficients on the sting support and plug surface. The solid line was found using the fully developed pipe flow equation (ref. 10) and the area-ratio method of calculating pressure distribution. The short-dashed line represents the results of the Bartz boundary-layer analysis (ref. 11), again, using the area-ratio method to calculate pressures. The Bartz method was also run using measured pressures on the supersonic side, and the results are plotted as the dashed line in figure 8. The Bresnahan data shown in figure 7 were used for the pressure distribution. The effect of the overexpansions and recompressions is clearly seen on the heat-transfer coefficient with variations as high as 30 percent from the constant pressure assumption.

The effect of using these different heat-transfer coefficients on wall temperature is seen in figure 9. The sharp temperature gradients on the subsonic side of the plug result from the changes in the number of fins along the passage. These spikes would be smoothed in the actual case by conduction in the wall, which was neglected in this study. Neglecting wall conduction should not change the average wall temperature. Comparison of the two curves using the Bartz coefficients indicates that the difference between the constant-pressure assumption and the variable-pressure assumption results in a wall-temperature difference of only about 56 K (100° R) - or about 4 percent. The pipe flow equation yields the highest coefficients that occur at the nozzle throat, and, therefore, yields the highest, most conservative, wall temperatures. For this reason, and since the pipe flow equation was much easier to work with, it was used to perform most of the calculations described in this report.

The results of the turbulent flat-plate equation shown in figure 8 were used to calculate the convective heat transfer to the film-cooled extension. The results from the flat-plate equation are in reasonably good agreement with the coefficients used on the convectively cooled portion of the plug, as expected.

Hot-gas temperature. - Another factor affecting the wall temperature is the radial hot-gas total-temperature profile. Figure 24 of reference 3 presents several gas-temperature profiles that were measured just downstream of the primary nozzle throat in the J-85-GE-13 engine plug nozzle tests. The profiles were similar in that each exhibited hotter gas temperatures at the center of the stream than near the plug surface or the primary nozzle lip. This was not a boundary-layer phenomenon, however, but was attributed to the annular burning pattern in the afterburner. As a result, some uncertainty exists as to which temperature to use as the driving temperature in the calculation of the

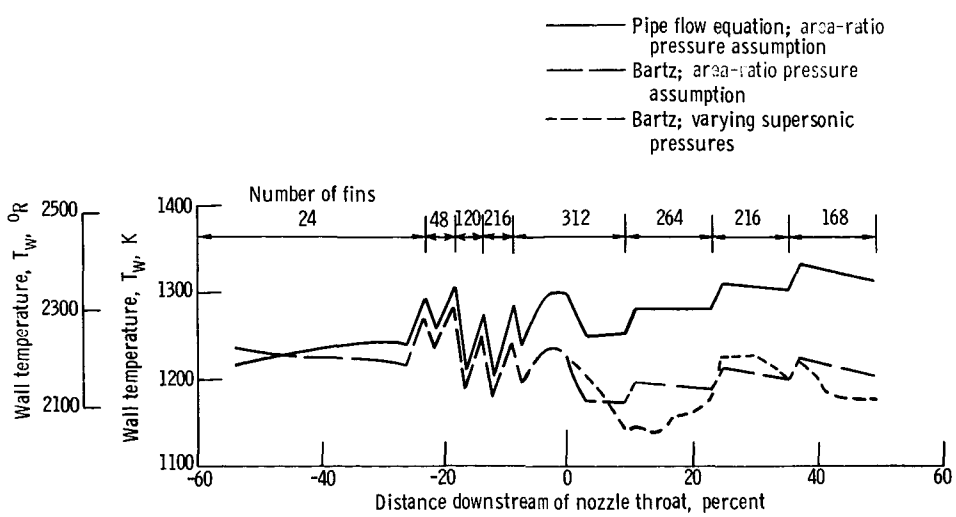

Figure 9. - Effect of heat-transfer coefficient on wall temperature. Sea-level takeoff; maximum afterburning; primary static temperature, 1945 K (3500° R); 2 percent coolant from compressor discharge.

heat transfer to the plug wall. It was decided to use both the average or bulk gas temperature and an estimate of the gas temperature near the plug wall, for this study. The measured gas temperatures near the plug wall, shown in figure 24 of reference 3, were cross plotted as a function of average gas temperature and a linear relation resulted. Extrapolation to an average total temperature of 1945 K (3500° R) resulted in a gas total temperature near the wall of about 1667 K (3000° R). Each of these two gas temperatures were used as the driving temperature in the calculations for this report.

Effect of coolant flow rate on wall temperatures. - Figure 10 shows the effect of varying the amount of cooling air on the plug wall temperatures. For this figure the pipe-flow equation was used to calculate the heat-transfer coefficients, and the area-ratio method was used to calculate local pressures and velocities. The air coolant for this figure was assumed to have been obtained after the last stage of the compressor (temperature, 667 K (1200° R), maximum pressure, 10.2 atm (150 psia)). In figure 10(a), it can be seen that less than 2-percent coolant is required to cool the plug below the maximum design wall temperature of 1220 K (2200° R), for a driving gas temperature of 1667 K (3000° R). In figure 10(b), for a driving gas of 1945 K (3500° R), about 3-percent coolant would be required to maintain wall temperatures below 1220 K (2200° R). Note that compressor discharge air was assumed for the coolant; if the pressure requirements are significantly lower than the available 10.2 atmospheres (150 psia), the air may be removed from an earlier stage on the compressor. The air temperature would then be reduced and the resulting wall temperatures could be reduced.

Coolant pressure requirements. - Figure 11 presents the calculated pressure requirements as a function of coolant flow rate and location of film cooling slot (i.e., the end of the convective-cooling passage and the beginning of the film-cooled extension). Again, the pipe flow equation was used to calculate the hot-gas heat transfer to the plug, and the area-ratio method was used to calculate pressure. The coolant was assumed to have been obtained from the compressor discharge. Figure 11(a) shows the calculated coolant total pressure at the end of the convective-cooling passages based on flow rate, area, and temperature. No data are shown for the 10-percent slot location for flow rates greater than 2.5 percent of the primary flow because the cooling air choked in the cooling passage, not at the end of the passage.

Figure 11(b) shows the calculated total pressure required at the inlet to the coolant channels. Minor losses between fin sections were shown to be small in the data of reference 3 and were, therefore, neglected. Also shown in the figure are the compressor-stage exit pressures. The results show that, if the plug were to be convectively cooled to the 75 percent point on the plug, cooling air would have to be obtained after the eighth stage of the compressor (3.5 percent coolant). It was decided, however, to incorporate some film-cooled portion of the plug in order to (1) recover some thrust from the heated coolant, (2) reduce the plug weight, and (3) reduce the plug pressure drop. For a coolant

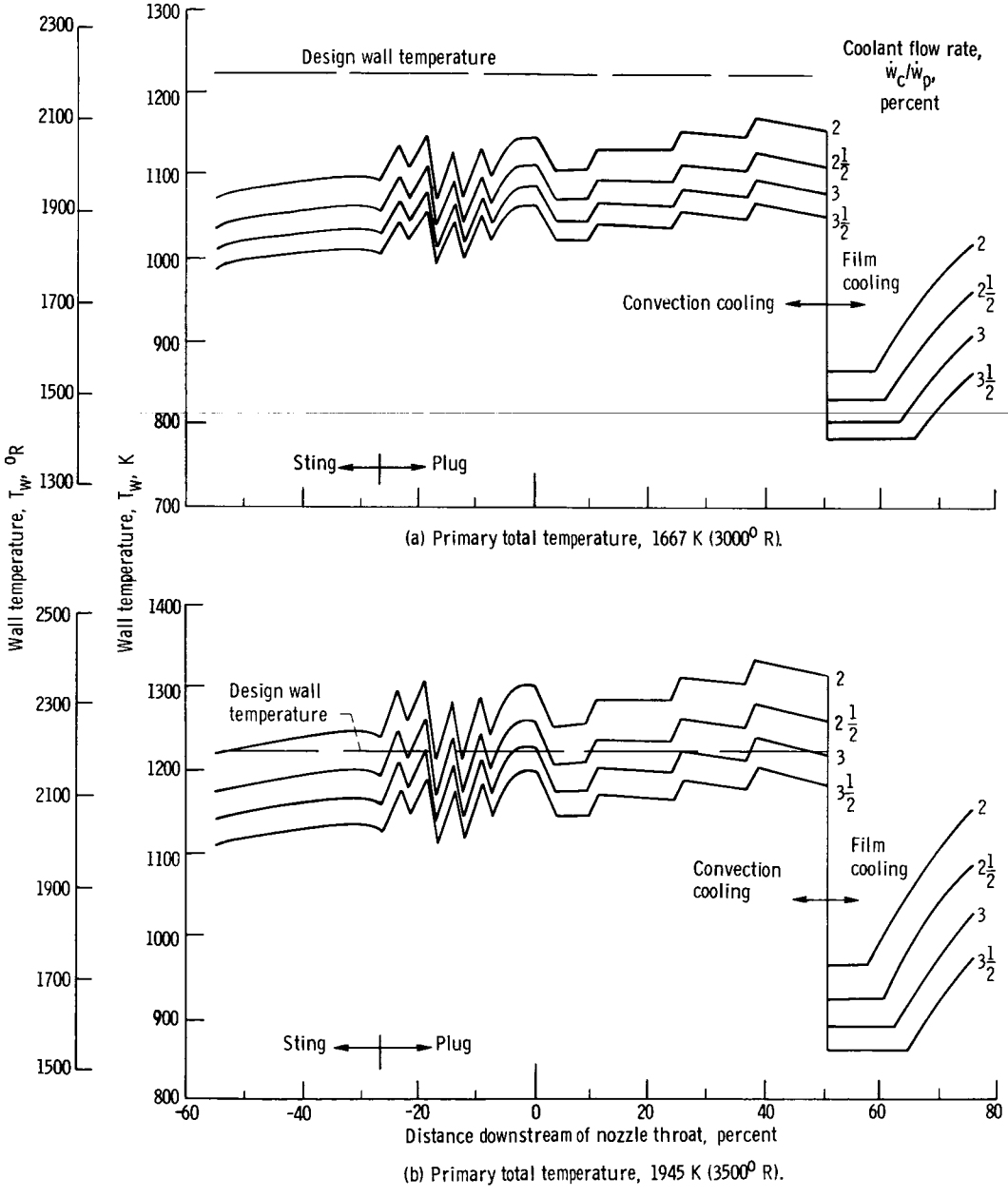

(a) Primary total temperature, 1667 K (3000° R).

(b) Primary total temperature, 1945 K (3500° R).

Figure 10. - Effect of coolant flow rate on plug wall temperature. Sea-level takeoff; Mach 0; pipe flow equation (compressor exit coolant); coolant inlet temperature, 667 K (1200° R); emissivity, 0.65.

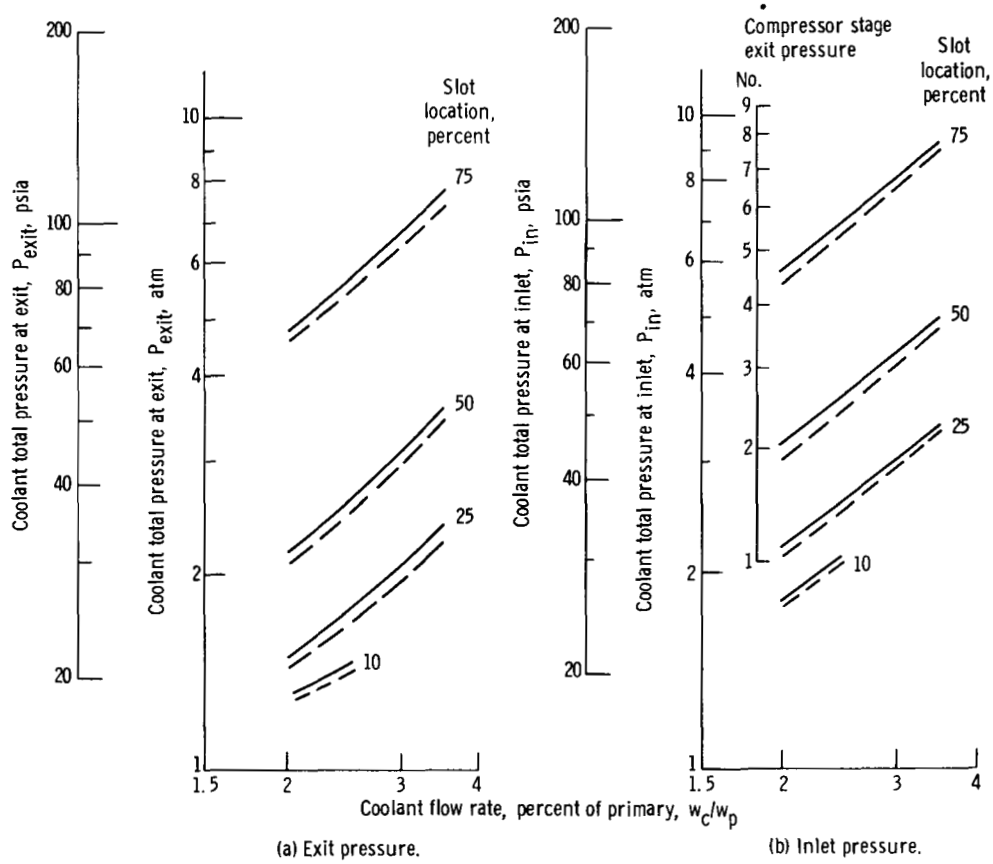

Figure 11. - Effect of coolant flow rate and slot location on coolant total pressure. Cooling air assumed to be taken from the end of the compressor. Sea-level takeoff; maximum afterburning.

discharge station at the 50-percent point on the plug, a compressor discharge port after the fourth stage would provide cooling airflow up to about 3.5 percent of the primary airflow. Similarly, a discharge port after the third stage would provide up to about 3 percent of the primary airflow; figure 10 indicated that 3-percent coolant would be the maximum required for the convectively cooled portion of the plug (T_p = 1945 K (3500° R)) and that the actual coolant required would probably be less than 2 percent (T_p = 1667 K (3000° R)).

If the end of the convective-cooling passages could be located at the 25-percent point on the plug, a discharge port after the second stage of the compressor would supply about 3-percent coolant to the plug. Similarly, for a plug with convection cooling to the 10 percent point and film cooling to the 75-percent truncation point, a compressor discharge port after the first stage of the compressor would supply about 2.5 percent of the engine primary airflow to the plug.

For coolant flow rates greater than 2.5 percent and the 10-percent slot location, the coolant chokes upstream of the convective-cooling-passage exit. In other words, the minimum area is no longer the exit, but the junction between the sting support and plug.

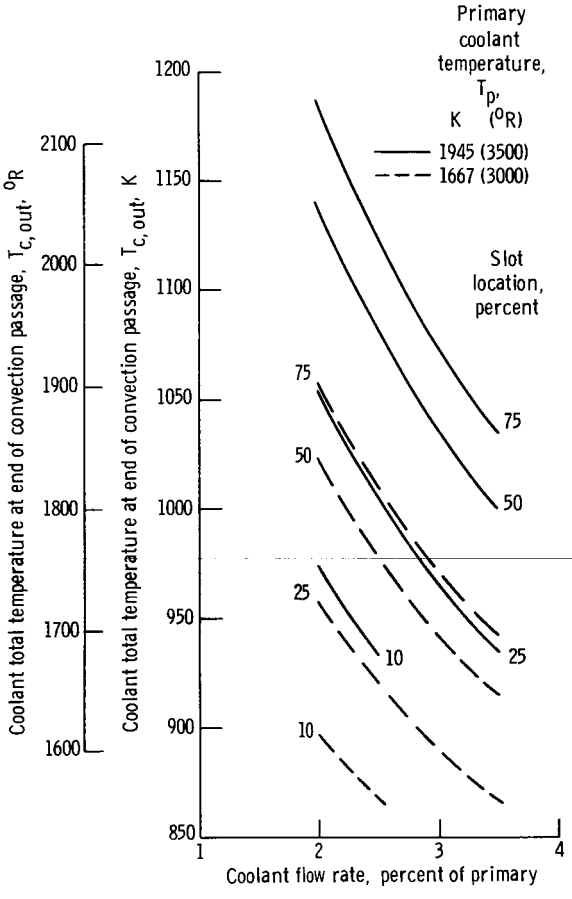

Figure 12. - Total temperature of coolant discharging from plug cooling channels. Sea-level takeoff; maximum afterburning cooling air obtained from end of compressor.

For this reason these portions of the curves are not shown in figure 11.

Temperature of coolant at film-cooling slot. - Let us now briefly discuss some of the cooling aspects of the film-cooled extension. Figure 12 presents calculated coolant total temperatures at the end of the convective-cooling passage. As in figure 10, the coolant was assumed to have been obtained from the end of the compressor (T = 667 K (1200° R)). These temperatures are required input for the film-cooling calculations and would be lower if cooling air can be taken from an earlier stage on the compressor, where the temperature is much lower.

Effect of coolant temperature and flow rate on film cooling. - Figure 13 shows the effect of cooling air temperature and flow rate on plug extension wall temperatures. The curves presented were calculated using hot-gas temperatures of 1945 K (3500° R) and 1667 K (3000° R), a nozzle pressure ratio of 3.0, and a film-cooled plug extension from the 10-percent point on the plug to the 75-percent truncation point. Only those portions

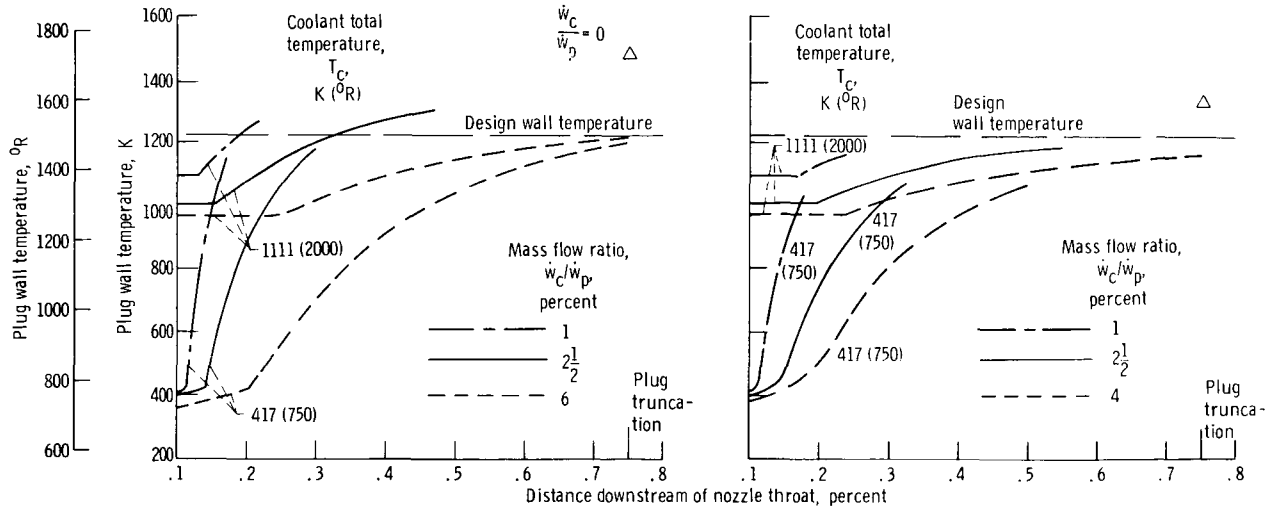

(a) Primary total temperature, 1945 K (3500° R).

(b) Primary total temperature, 1667 K (3000° R).

Figure 13. - Effect of coolant total temperature and coolant flow rate on plug extension wall temperature. 10-Percent slot; wall emissivity, 0.65. Curves are shown within range of data correlation (ref. 6).

of the curves within the range of the film-effectiveness data correlation of reference 6 are shown.

For a 6-percent coolant flow rate (fig. 13(a)) the plug wall temperature is approximately the same at the end of the plug, whether the coolant total temperature was 417 K (750° R) or 1111 K (2000° R). For the 2.5- and 1-percent coolant flow-rate cases, the maximum design wall temperature will apparently be exceeded. Thus, it appears that lowering the coolant total temperature will have little effect on plug extension maximum wall temperatures for this application, except in the immediate vicinity of the film-injection slot. The effect of an increase in coolant flow rate, however, is characterized by a shifting of the wall-temperature curves downward and to the right. It appears from figure 13(a) that about 6 percent of the engine primary flow is required to film cool an extension from the 10-percent point to the 75-percent truncation point using cooling air obtained at the end of the compressor and assuming that the total gas temperature is 1945 K (3500° R). Six percent cooling air is too high to maintain high cycle efficiency; therefore, using the 10-percent slot is impractical for these conditions. Similarly, a slot further upstream would require even more cooling air and for that reason was not considered in this study.

If the effective primary total temperature is assumed to be 1667 K (3000° R), then the use of the 10-percent coolant slot position does appear possible. Figure 13(b) shows that the wall temperature will be approximately equal to the design wall temperature. Most of the wall cooling is being accomplished by wall-to-ambient radiation. The symbol shown in figure 13 indicates the wall temperature that would result with no film-cooling air ($\dot{w}_c/\dot{w}_p = 0$); all cooling would be accomplished by radiation.

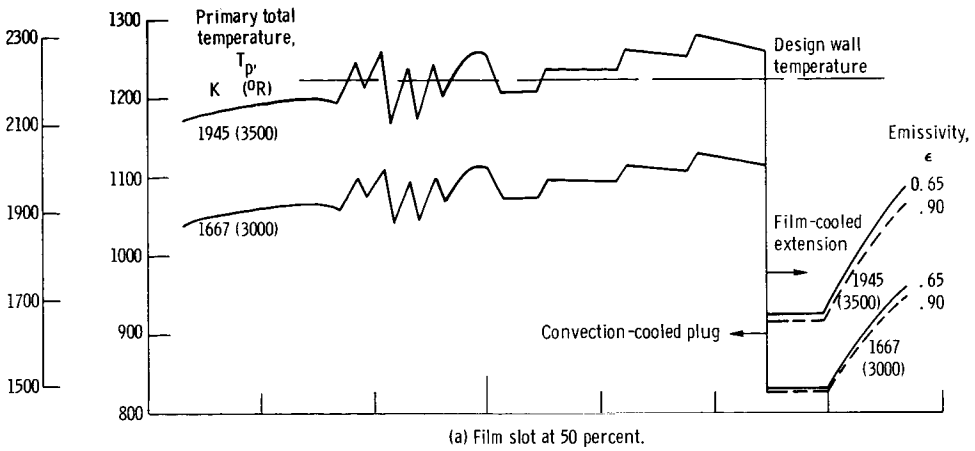

(a) Film slot at 50 percent.

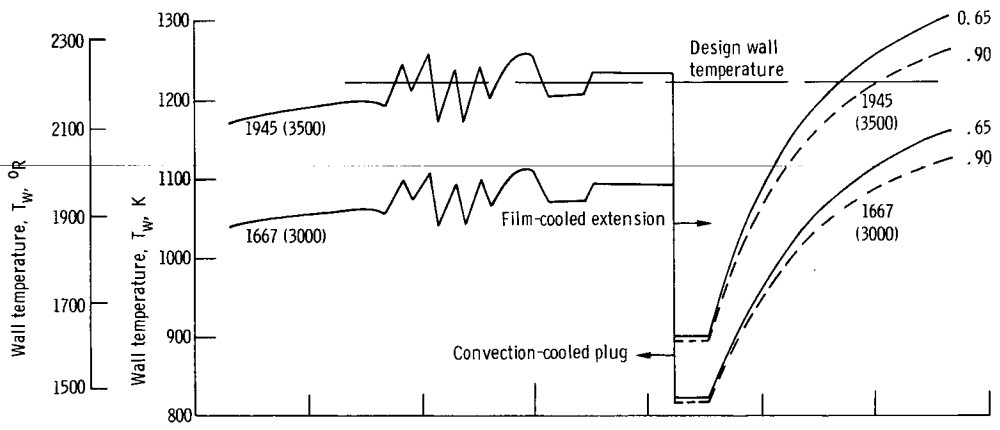

(b) Film slot at 25 percent. Support test data on film cooling (ref. 6) were unavailable for this slot location.

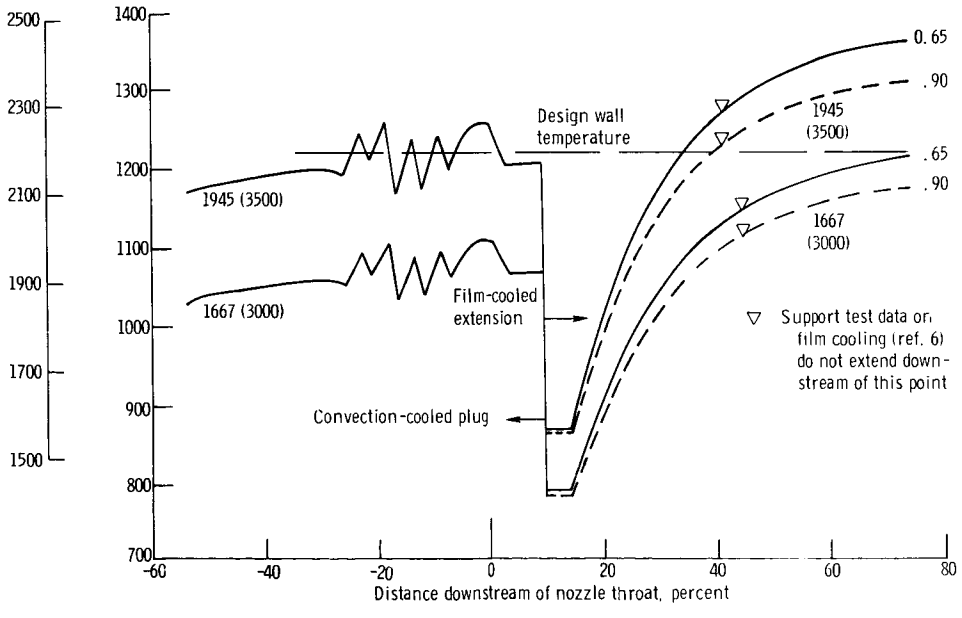

(c) Film slot at 10 percent.

Figure 14. - Film-cooled plug extension temperatures. Sea-level takeoff; maximum afterburning; mass flow ratio, $2\frac{1}{2}$ percent; cooling air from end of compressor.

Effect of slot location on wall temperatures. - Figure 14 shows the effect on wall temperature on film-cooling slot location using cooling air obtained at the end of the compressor. Figure 14(a) shows the results of convection cooling to the 50-percent point on the plug and film cooling to the 75-percent truncation point. Figure 14(b) shows the results of convection cooling to the 25-percent point, and figure 14(c) shows the results for convection cooling to the 10-percent point. Two and one-half percent of the primary air was assumed for this figure, and the pipe flow equation was used to calculate the heat-transfer coefficients to the convectively cooled portion of the plug. Figure 14 shows, for the convectively cooled portion, that an effective gas temperature of 1945 K (3500° R) results in a marginal design with a maximum wall temperature of about 1258 K (2265° R) at the nozzle throat. Using an effective gas temperature of 1667 K (3000° R), which is probably more realistic, reduces the nozzle throat wall temperature to about 1111 K (2000° R).

The film-cooled extension temperatures for the case with film cooling from the 50-percent point are well below the design temperature limit of 1222 K (2200° R). The effect of wall emissivity ϵ_w is small over the expected range for the materials involved. The film-cooled wall temperatures for the slot located at the 25-percent point are shown in figure 14(b). These temperatures are marginal for the 1945 K (3500° R) gas temperature but adequate for the 1667 K (3000° R) gas temperature. Similarly, the wall temperatures with convection cooling to the 10-percent point on the plug (fig. 14(c)) appear to be too high for the higher gas temperature but reasonable for the lower gas temperature.

Now, consider what would happen to these extension temperatures if lower temperature cooling air could be used to cool the plug (from an earlier compressor stage, for example). It was shown in figure 13 that coolant-inlet temperature had little effect on maximum extension temperature for a coolant slot located at the 10-percent point because the downstream film effectiveness was small and most of the cooling was accomplished by radiation. Therefore, reducing the coolant-inlet temperature would not significantly reduce the maximum-extension wall temperature for the 10-percent slot case. The same reasoning applies for the slot at the 25-percent point. On the other hand, the configuration with the extension located at the 50-percent point would be favorably affected by a reduction in coolant-inlet temperature because of the short length of the film-cooled portion.

Resulting wall temperatures using interstage compressor bleed. - The cooling requirements for the sea-level-takeoff flight condition are summarized in figure 15. The experimental pressure distribution of Bresnahan (ref. 7) was used on the supersonic side of the plug to calculate local Mach numbers. Then the Bartz boundary-layer method was used to calculate gas-to-wall convection heat transfer. These assumptions are believed to be the most realistic for final calculations. The curves shown were calculated using the higher gas temperature, 1945 K (3500° R). Obviously, lower wall temperatures would result if the lower gas temperature were used. The lower curve was calculated

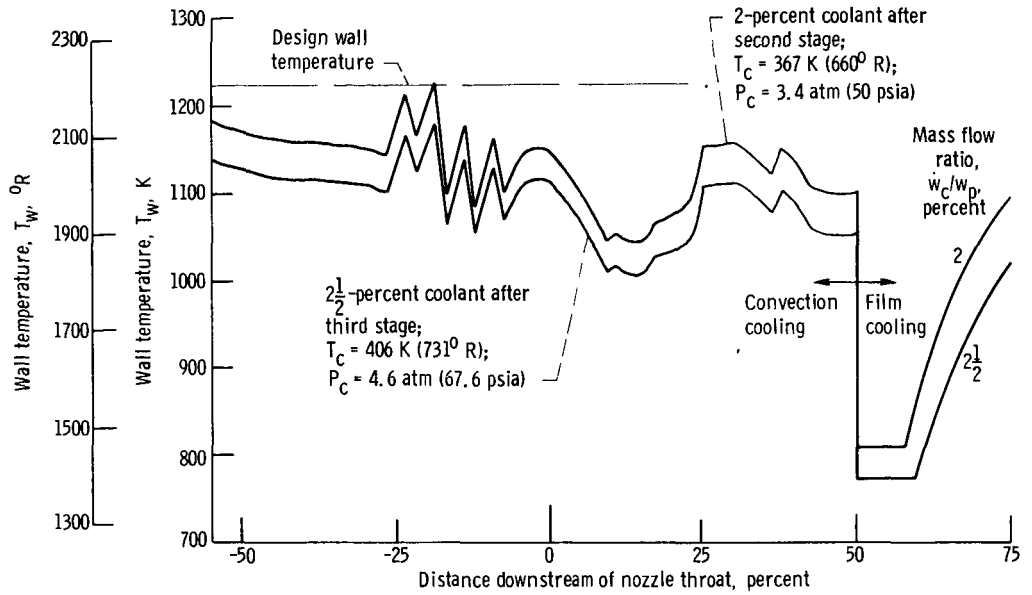

Figure 15. - Resulting wall temperatures using compressor interstage bleed. Sea-level takeoff; maximum afterburning, primary total temperature, 1945 K (3500° R).

using 2.5 percent of the primary airflow to cool the plug and sting support, removed after the third stage of a nine-stage compressor. The temperature of the cooling air at this stage is only 406 K (731° R), and the pressure is 4.60 atmospheres (67.6 psia). The calculated total pressure required at the inlet to the sting support is only about 3.28 atmospheres (48.2 psia); therefore, 1.32 atmospheres (19.4 psia) are available to duct the air from the compressor to the sting support inlet. Since these wall temperatures are well below the maximum wall temperature, this configuration is feasible.

The upper curve in figure 15 was calculated using 2 percent of the primary airflow removed after the second stage of the compressor. The temperature and pressure of the air available at this point are 367 K (660° R) and 3.4 atmospheres (50 psia), respectively. The calculated pressure required at the inlet to the sting support for this configuration is only 2.72 atmospheres (40.0 psia). Again, 0.68 atmosphere (10. psia) is available between the compressor bleed port and the sting support inlet. These wall temperatures are also well below the maximum wall temperature, so this configuration also appears to be practical. The film-cooled extension temperatures are also satisfactory. Since there are performance gains to be made from removing this air from as early a stage as possible, the latter configuration would be favored.

Supersonic Cruise

Upon selecting a cooling configuration for one flight condition (takeoff, in this case),

it becomes necessary to evaluate the cooling requirements at other flight conditions. The supersonic-cruise condition assumed for this study included a flight Mach number of 2.7, a primary flow rate of 186 kilograms per second (410 lbm/sec), a nozzle total pressure of 1.97 atmospheres (29 psia) at beginning of cruise and 1.35 atmospheres (20 psia) at end of cruise, and a nozzle pressure ratio of 27.6. The afterburner was presumed to be on at a low power setting, resulting in a nozzle total temperature that varied from 1347 to 1286 K (2425° to 2314° R) from the start of cruise until the end of cruise, respectively. The primary nozzle flow area was reduced from 10 600 square centimeters (1642 in.^{2}) for maximum afterburning to 8500 square centimeters (1317 in.^{2}) at supersonic cruise.

Plug static pressure distribution. - Figure 16 shows measured plug static pressures for 10° half-angle conical plugs operating at high pressure ratios. The Bresnahan data (ref. 7) were obtained on a 12.24-centimeter (4.82-in.) plug diameter model in both a wind tunnel and in a static-test facility. The location shown for the end of the cylindrical ejector for these data is approximately optimum for this nozzle pressure ratio. No secondary flow was used for the data shown, however. The Huntley data (ref. 4) were obtained from an uncooled plug attached to an afterburning turbojet; the engine could only be operated in the nonafterburning mode, however, because of the temperature limit on the uncooled plug. The corrected secondary weight flow ratio was 6.3 percent for these data, and the secondary shroud location was not optimized. The Clark data (ref. 3) were obtained on a cooled plug with nonafterburning for the case shown. The cylindrical ejector

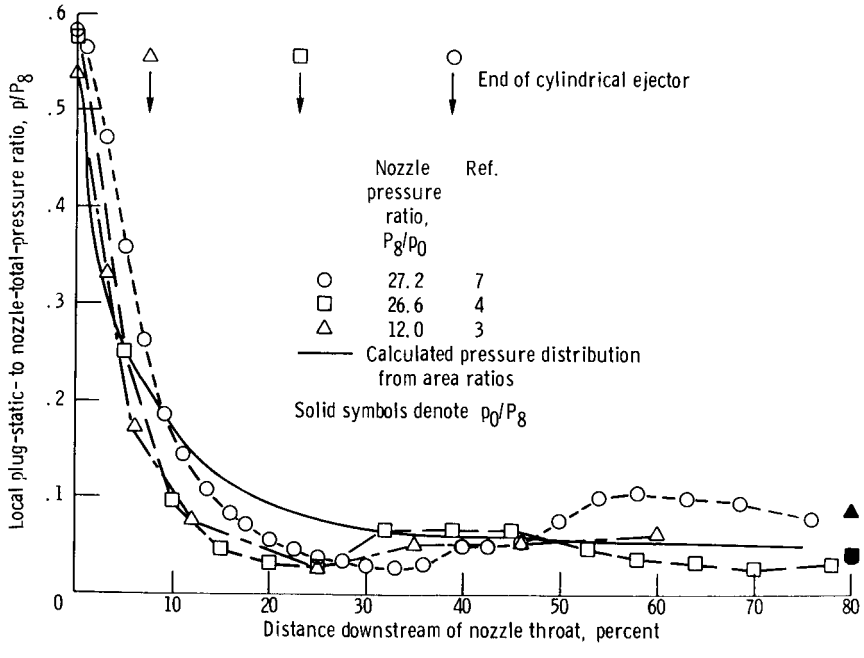

Figure 16. - Comparison of predicted and experimental pressures on plug surface. Supersonic cruise; Mach 2.7.

position was not optimized for the nozzle pressure ratio. Secondary air was used, however.

The calculated pressure distribution, using the approximate, area-ratio method, yields reasonable results up to about the 10-percent point on the plug and between the 30-percent point and the 50-percent point. From about the 10-percent point to the 30 percent point, the estimate is too high, by a factor of about 2 at the 25-percent point.

Comparison of predicted heat-transfer coefficients. - Figure 17 compares the various methods used to predict heat-transfer coefficients for the supersonic-cruise flight

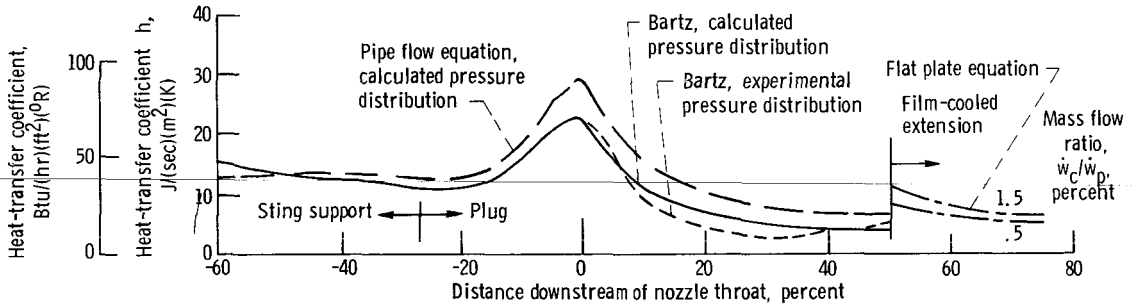

Figure 17. - Comparison of heat-transfer coefficients. Supersonic cruise; primary total temperature, 1345 K (2425° R); Mach 2.7; coolant total temperature, 533 K (960° R).

regime. The dashed line in figure 17 shows the coefficients using the pipe flow equation and pressures using the area-ratio method. The solid line on figure 17 was found by using the Bartz method, again using the area-ratio method of predicting pressures. The short-dashed line in the figure was calculated using the Bartz method and the experimental pressures of Bresnahan (see fig. 16) to evaluate the error introduced by using the area-ratio method of calculating pressures. Comparison of the two Bartz curves shows that the heat-transfer coefficient distribution is similar to the pressure distribution assumed. Also, the pipe flow equation predicts a higher heat-transfer coefficient over the entire plug. Therefore, the use of the pipe-flow equation should yield a conservative design.

Effect of hot-gas temperature profile. - A hot-gas temperature profile will exist in the primary gas stream even for the low level of afterburning assumed (see ref. 3). The relation found from reference 3 between average gas temperature and gas temperature near the wall yields, for an average gas temperature of 1347 K (2425° R), a gas temperature near the plug of about 1166 K (2100° R). Thus, if the afterburner burner profile found on the J-85-GE-13 afterburning turbojet of reference 3 can be duplicated on the larger supersonic-cruise aircraft, no plug cooling will be required for supersonic cruise, and plug wall temperatures will be about 1166 K (2100° R). In the discussion that follows

an average gas temperature of 1347 K (2425° R) is assumed to be the driving temperature, and the cooling air is assumed to have been obtained from the engine inlet with a ram pressure of 1.52 atmospheres (22.3 psia) and temperature of 533 K (960° R).

Ram-air coolant requirements. - Figure 18 summarizes the effect of ram-air coolant flow rate on both plug wall temperature at the primary throat and calculated plug-inlet coolant pressure. The abscissa shows the coolant flow rate as a percent of the engine primary airflow and the right ordinate is a measure of the required inlet pressure at the cooling passage inlet station. The left ordinate shows plug wall temperature at the

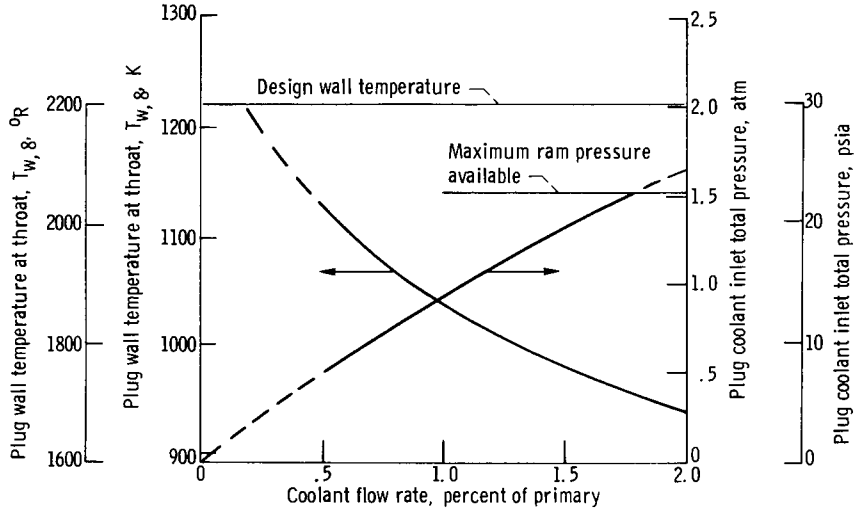

Figure 18. - Effect of coolant flow rate on plug throat wall temperature and required coolant inlet pressure. Supersonic cruise point; primary total temperature, 1345 K (2425° R). Mach 2.7; ram cooling air; coolant total temperature, 533 K (960° R).

nozzle throat (station 8). The calculations were made using the area-ratio method to calculate pressures on the supersonic side; heat-transfer coefficients were calculated using the pipe flow equation.

The figure indicates that about 1.5 percent of the primary airflow may be obtained using a ram inlet and that this flow would result in a plug wall temperature at the primary throat of about 978 K (1760° R). Restricting the flow would result in higher wall temperatures, but a flow rate as low as 0.5 percent results in a temperature of only about 1128 K (2030° R) - well below the design wall temperature of 1222 K (2200° R). Obviously, the selection of the correct flow rate for this flight condition will also include a life criteria; lower temperatures generally result in longer lives. Operation with the coolant flow rate between 0.5 and 1.5 percent of primary flow would result in plug temperatures between the two curves in figure 19, which should yield satisfactory life.

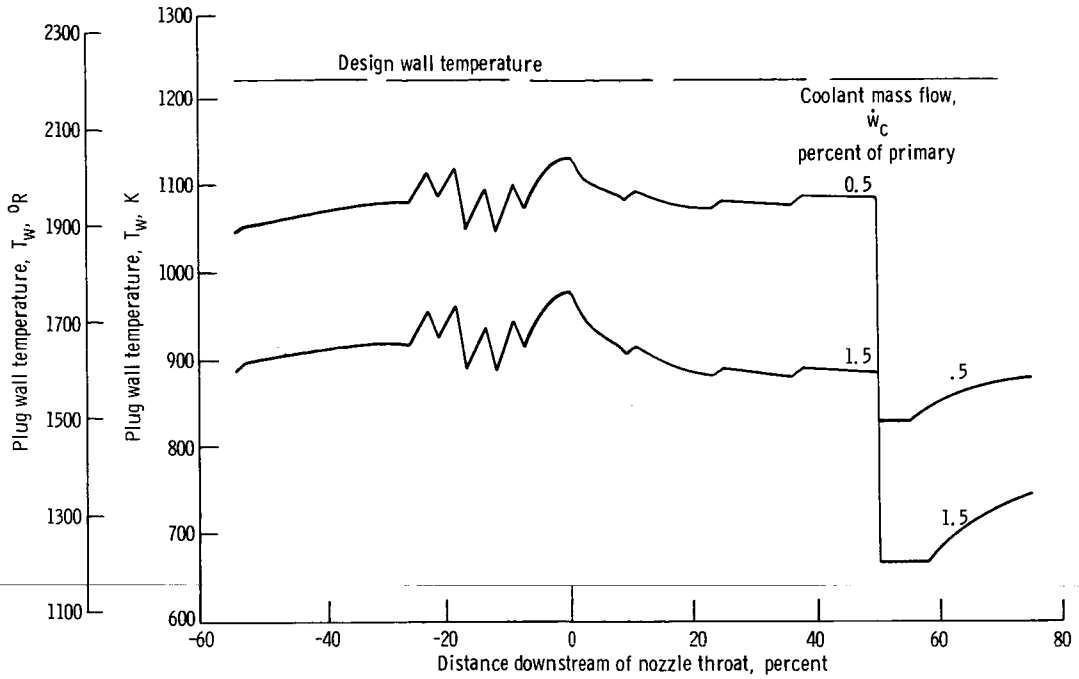

Figure 19. - Wall temperatures at supersonic cruise. Primary total temperature, 1345 K (2425° R); Mach 2.7; ram air coolant; pipe flow equation.

Maximum Acceleration

Figure 20 compares plug wall temperature at the nozzle primary throat for the entire Mach number range up to 2.7 for maximum afterburning. Two-percent coolant was assumed to have been taken from the engine after the second stage of the compressor. For these calculations, local velocity and pressure were found using the area-ratio method, and heat-transfer coefficients were calculated using the pipe flow equation. The figure shows that the maximum plug wall temperature $T_{w,8}$ will be below the design temperature except for takeoff and above Mach 1.85 for the 1945 K (3500° R) curve. When the gas temperature profile is taken into account (the 1667 K (3000° R) curve in fig. 20), the maximum plug wall temperature is predicted to be below 1162 K (2093° R). Actually, on a typical mission, the pilot would throttle the afterburner back as he approached Mach 2.7, thus reducing the plug wall temperature. It appears that 2-percent coolant, removed from the compressor after the second stage, should provide adequate plug cooling during maximum afterburning.

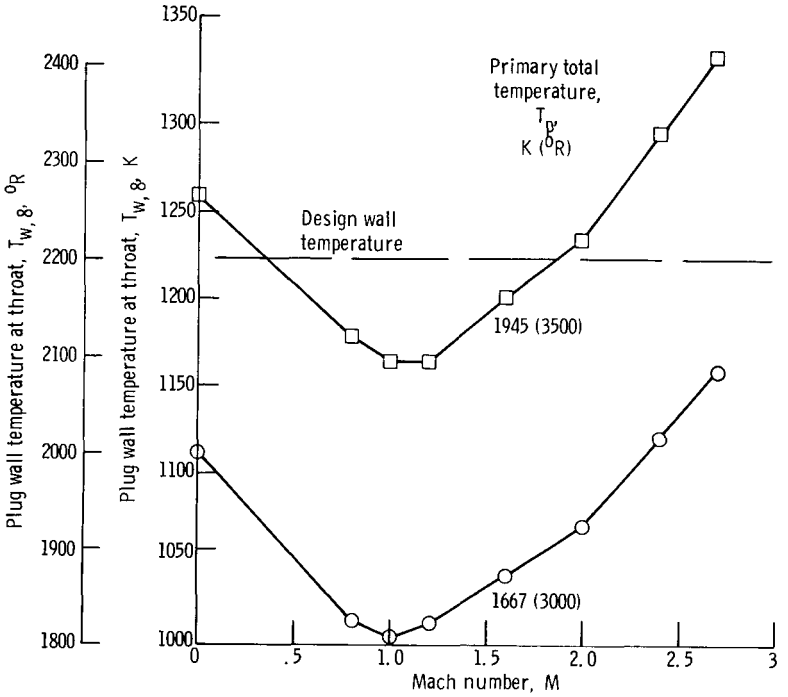

Figure 20. - Plug throat wall temperature as function of Mach number. Maximum afterburning; 2 percent coolant from compressor second stage.

OTHER CONSIDERATIONS

As discussed in the INTRODUCTION of this report, certain other considerations are important in a nozzle design. The plug weight, assuming convection cooling to the 50 percent point, was calculated by considering the outer wall, fins, and inner wall and was found to be about 616 kilograms (1361 lbm). For four engines this is about 0.7 percent of the entire aircraft weight. Breaking this weight down into the various components:

Plug and sting support outer wall, kg (lbm)	219 (482)
Plug and sting support inner wall, kg (lbm)	56 (123)
Plug and sting support fins, kg (lbm)	315 (694)
Upstream of primary throat, kg (lbm)	81 (178)
Downstream of primary throat, kg (lbm)	219 (482)
Sting support, kg (lbm)	15 (34)
Film-cooled extension, kg (lbm)	26 (57)
Total, kg (lbm)	616 (1361)

Notice that about 35 percent of the weight is in the fins downstream of the primary throat. Thus, if the convective cooling passage ended at the 25-percent point and the plug extension would film cool to the 75-percent truncation point, about 100 kilograms

(221 lbm) could be saved per engine. Similarly, if the extension would film cool all the way from the 10-percent point to the 75-percent point, about 186 kilograms (410 lbm) could be saved per engine.

Lateral vibration was checked using the method of reference 12. The method assumes that the first natural frequency in the lateral mode can be found by assuming that the sting support extends to the center of gravity of the plug and that the mass of the plug is concentrated at the center of gravity. Also, 23.6 percent of the weight of the sting support is assumed to be concentrated at the plug center of gravity as outlined in the method of reference 12. Young's modulus was assumed to be 1.59×10^{11} newtons per square meter (23.1×10^{6} psi), and the moment of inertia of the sting, including the fins, was calculated to be 21 500 cm^4 (517 $in.^4$). Thus, the first natural frequency was calculated to be 6.65 hertz.

Stresses in the support tube wall were checked using elementary strength of materials theories. The longitudinal stress caused by an internal pressure of 3.45×10^{5} newtons per square meter (50 psi) is 1.38×10^{7} newtons per square meter (2000 psi). The circumferential stress resulting from the same internal pressure is 2.76×10^{7} newtons per square meter (4000 psi). Bending stress was calculated by assuming an equivalent static load at the plug center of gravity resulting from an acceleration of four gravities. The maximum bending stress at the junction with the turbine frame was found to be 5.86×10^{7} newtons per square meter (8500 psi). This stress combines with the longitudinal stress to yield a maximum tensile stress of 7.24×10^{7} newtons per square meter (10 500 psi). Thus, to maintain a 1000-hour rupture strength, the temperature of the wall at this point must be kept below about 1110 K (2000° R). Similarly, the bending stress was checked at the junction between the sting support and the plug. The bending stress was found to be 3.38×10^{7} newtons per square meter (4900 psi), and the total tensile stress 4.76×10^{7} newtons per square meter (6900 psi). Based on the calculated wall temperature of about 1166 K (2100° R) (see fig. 15) at this point, the rupture life should be between 100 and 1000 hours. This life can be improved by improving the cooling in this area or by building stiffeners into the sting support.

Buckling of the support tube wall was also checked and was not found to be a problem.

The purpose of these preliminary stress calculations was to determine whether or not the wall size selected was reasonable. The numbers indicate that it is.

SUMMARY OF RESULTS

The important results of this thermal design study may be summarized as follows:

1. An air-cooled plug-nozzle system for an afterburning turbojet engine for a supersonic-cruise aircraft appears to be practical using low-cycle-penalty cooling air.

During maximum afterburning (i.e., sea-level takeoff and acceleration up to Mach 2.7), 2 percent of the primary airflow may be removed after the second stage of a nine-stage compressor and should result in plug wall temperatures below 1222 K (2200° R).

2. During supersonic-cruise operation, ram air may be used to cool the plug and sting support. About 1.5 percent of the primary airflow may be obtained at ram pressure and temperatures, which would result in maximum plug wall temperatures of about 978 K (1760° R), when it is assumed that the average gas temperature is the driving temperature. Restricting the coolant flow to about 0.5 percent would result in maximum wall temperatures of about 1133 K (2040° R). If the hot-gas temperature profile can be tailored so that the gas temperature near the plug wall is below 1222 K (2200° R), then no cooling air should be required during supersonic cruise.

3. The configuration selected includes a 10° half-angle plug that is sting supported to the turbine frame. Convection cooling on the sting support and plug up to the 50-percent point on the plug (half-way between the primary nozzle and the end of a full plug) should provide adequate cooling with low pressure drop. At the 50-percent point, the air coolant would be injected as a film over a 10° half-angle extension that is truncated at the 75-percent point. Thus, some thrust may be recovered from the heated coolant.

4. Preliminary stress calculations indicate that the wall size selected is reasonable. The plug weight was calculated to be about 616 kilograms (1361 lbm) for a plug with convection cooling to the 50-percent point and film cooling to the 75-percent point. Lateral vibration of the plug was checked for this configuration, and the first natural frequency of the plug was found to be 6.65 hertz.

5. A configuration that includes convection cooling to the 10-percent point on the plug and film cooling to the 75-percent point also appears practical if the afterburner temperature profile can be tailored so that the driving temperature near the plug wall can be maintained at 1667 K (3000° R). This configuration would have a 186 kilograms (410 lbm) weight advantage over the configuration with convection cooling to the 50-percent point.

Lewis Research Center,
National Aeronautics and Space Administration,
Cleveland, Ohio, October 14, 1971,
764-74.

APPENDIX A

SYMBOLS

A	area
A^*	critical area
a	absorptivity
a_{gw}	absorptivity of gas from a source at T_w
C	correction factor in radiation (eq. (C6))
C_D	discharge coefficient, Actual flow/Ideal flow
C_p	specific heat at constant pressure
D	diameter
D_h	hydraulic diameter
F	radiation configuration factor
f	friction factor
f/a	fuel-air ratio
G	specific flow rate, $\dot{w}/A$
g	Newton's conversion constant
H	fin height
H'	length of equipotential line (i. e., passage height)
h	heat-transfer coefficient
I	station index
J	Joule's constant
k	thermal conductivity
L	length
L_b	mean beam path length
M	Mach number
P	total pressure
Pr	Prandtl number
p	static pressure
p'	partial pressure
q	heat-transfer rate per unit area
R	gas constant
Re	Reynolds number
R_i	inner radius of hot-gas flow channel
R_o	outer radius of hot-gas flow channel
S	film-cooling step height
Sp	fin spacing
T	total temperature
T_w	wall temperature
T'_w	adiabatic wall temperature
T_{rec}	recovery temperature
t	static temperature
V	velocity
W	fin base width
$\dot{w}$	mass flow rate
X	distance along plug surface downstream of slot
x	distance from base of fin
α	thermal diffusivity
γ	ratio of specific heats
ϵ	emissivity

Λ	recovery factor
μ	dynamic viscosity
ρ	density
σ	Stefan-Boltzman constant
τ	thickness

Subscripts:

am	ambient radiation conditions
av	average
c	coolant
co	carbon dioxide
conv	convection
eff	effective
exit	convective passage exit (coolant slot)
f	film
fl	flame
fin	fin
fr	friction
I	station index
i	inside
in	inlet to convective cooling slot
m	momentum
max	maximum
out	outside
p	primary
pl	plug
r	radiation
ref	reference properties
sl	coolant slot
w	wall
wa	water vapor
X	distance along plug surface downstream of slot
1	hot-gas-to-wall radiation
2	wall-to-coolant forced convection
3	wall-to-ambient radiation
8	primary nozzle station
0	ambient flow conditions

APPENDIX B

CONVECTION HEAT-TRANSFER AND PRESSURE-DROP ANALYSIS

The procedure used to analyze the plug-nozzle system was developed into two computor programs (FORTRAN IV): One program was used for the convection-cooled portions of the sting support and plug, and the second program analyzed the film-cooled plug extension (appendix C). The program used for the convection-cooling analysis assumes one-dimensional, steady-state heat flow through the outer wall and fins into the coolant. Transport properties of the hot gas were obtained from reference 13. A fuel-air ratio of 0.0566 was used for the maximum afterburning cases and 0.02 was used for supersonic cruise.

Input Data

The heat-transfer model used for the convection-cooled portion of the sting support and plug is shown in figure 6(a). The thermal conductivity of the outer wall and fins were assumed to be constant:

$$k_w = 32.9 \text{ J/(sec)(m)(K)} \ (19. \text{ Btu/(hr)(ft)}(^{\circ}\text{R}))$$

for a typical high strength nickel-base alloy and

$$k_{fin} = 55.3 \text{ J/(sec)(m)(K)} \ (32. \text{ Btu/(hr)(ft)}(^{\circ}\text{R}))$$

for nickel. The cooling passages were divided into equal 5.08-centimeter (2.0-in.) increments, and station calculations were performed on each increment. Coolant inlet total temperature and flow rate, hot-gas total conditions, and plug geometry were input to the program.

Heat Flux Loop

An energy balance was performed at each station that resulted in an estimate of the local wall temperature.

Coolant side. - At each station the following parameters were calculated: (1) Fin spacing, (2) coolant flow area, (3) coolant flow perimeter, (4) hydraulic diameter, (5) Reynolds number, and (6) heat-transfer coefficient. The coolant transport properties

were approximated from air tables as a function of the coolant total temperature. The coolant flow was turbulent for all conditions studied. The Dittus-Boelter correlation for turbulent flow (ref. 14) was used to calculate heat-transfer coefficients

$$h_{c,I} = \frac{k}{D_{h,I}} \left(0.023\ Re_{c,I}^{0.8} Pr^{0.4}\right) \tag{B1}$$

The effect of the high-conductivity fins was included by solving the one-dimensional conduction equation with the following boundary conditions (ref. 15):

(1) The temperature at the base of the fin is constant and equal to $T_{w,i}$.

(2) The temperature gradient at the end of the fins is zero ($dT/dx = 0$).

(3) The heat-transfer coefficient is constant and the same on the inner wall and fins.

The effective heat-transfer coefficient on the coolant side can be shown to be

$$h_{eff,c,I} = \frac{h_{c,I}}{Sp} \left[\frac{2 \tanh \left(H \sqrt{\frac{2h_{c,I}}{k_{fin} \tau_{fin}}} \right)}{\sqrt{\frac{2h_{c,I}}{k_{fin} \tau_{fin}}}} + (Sp - \tau_{fin}) \right] \tag{B2}$$

Hot-gas side. - On the hot-gas side the local calculated area ratios were used to calculate local hot-gas conditions assuming a specific heat ratio of 1.3 (ref. 16). In the subsonic region of the nozzle, this method was believed to yield a good prediction of hot-gas static pressure, static temperature, local velocity, and density. Problems develop in the supersonic region, however. The flow and, hence, pressure field in the supersonic region of the nozzle is a function of

(1) Nozzle pressure ratio

(2) Secondary shroud position

(3) Secondary airflow rate

(4) Primary gas flow rate

(5) Temperature of primary and secondary streams.

A method has been developed at Lewis to evaluate the performance of a fully expanded plug nozzle with secondary flow (ref. 1). A comparison of static pressures - experimental and predicted - is shown in reference 3. The program was developed for very high pressure ratios, that is, fully expanded flow. There is no known method for accurately predicting pressure distributions (and, hence, local velocities) for the lower pressure ratio cases. Therefore, a method was required for this study to evaluate the

lower pressure ratio cases (nozzle pressure ratio is shown in fig. 1(b) as a function of flight Mach number and varies from 3 to about 27).

The prediction method selected for this study yields, at best, a rather crude approximation of the local pressure distribution. The technique requires a guess at the flow boundary between the primary and secondary streams. Specifically, a drawing was made of the plug, primary nozzle lip, and secondary shroud. Then, the flow boundary between the primary stream and the secondary stream was estimated and sketched on the figure. Figure 21 shows the sketch for this nozzle. Equipotential lines were then estimated and drawn from the plug stations to the outer flow boundary. The secondary shroud diameter was assumed to be the outer limit of the equipotential lines, even downstream of the end of the secondary shroud. Outer radius and passage height were then scaled from the drawing, and the local area ratio was calculated.

$$\frac{A_I}{A^*} = \frac{\pi(R_i + R_o)H'}{A_8} \tag{B3}$$

Figure 21(b) shows the equipotential lines estimated for the supersonic side of the nozzle. This estimate was simply a first approximation; a check was made of the calculated local static pressure to be sure it was above the back pressure. For the low-nozzle-pressure ratio cases, the calculated static pressure dropped below the back pressure at some station along the plug downstream of the primary nozzle lip. When this occurred, the local pressure was set equal to the back pressure, and the area ratio was set equal to the maximum for this pressure ratio:

$$\left(\frac{A_8}{A}\right)_{max} = M\left[\frac{\left(\frac{\gamma+1}{2}\right)}{1+\left(\frac{\gamma-1}{2}\right)M^2}\right]^{(\gamma+1)/2(\gamma-1)} \tag{B4}$$

where

$$M = \sqrt{\frac{2}{\gamma-1}\left[\left(\frac{P_8}{p_0}\right)^{(\gamma-1)/\gamma} - 1\right]} \tag{B5}$$

Then, the local outside radius, passage height, and hydraulic diameter were recalculated

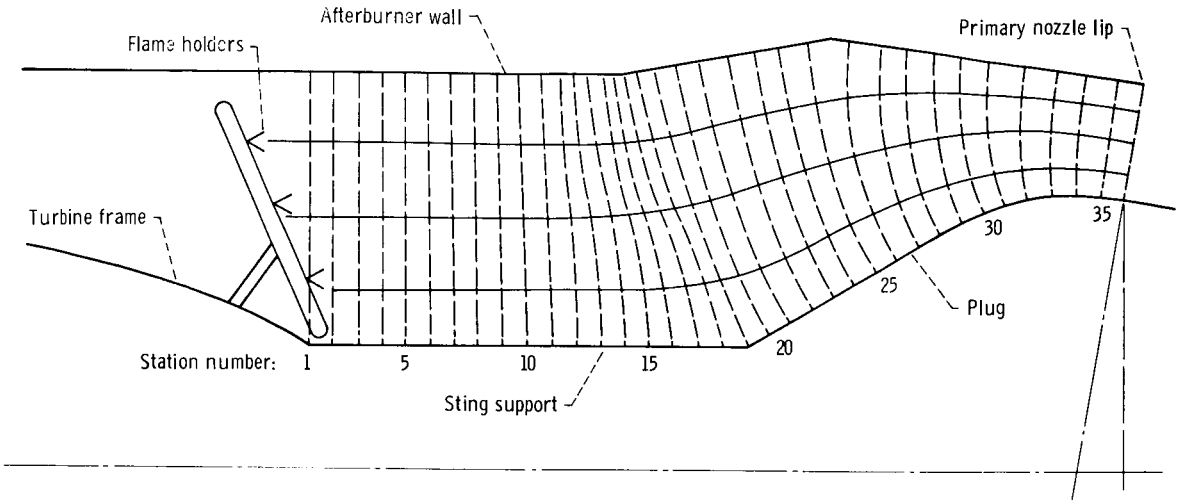

(a) Subsonic region.

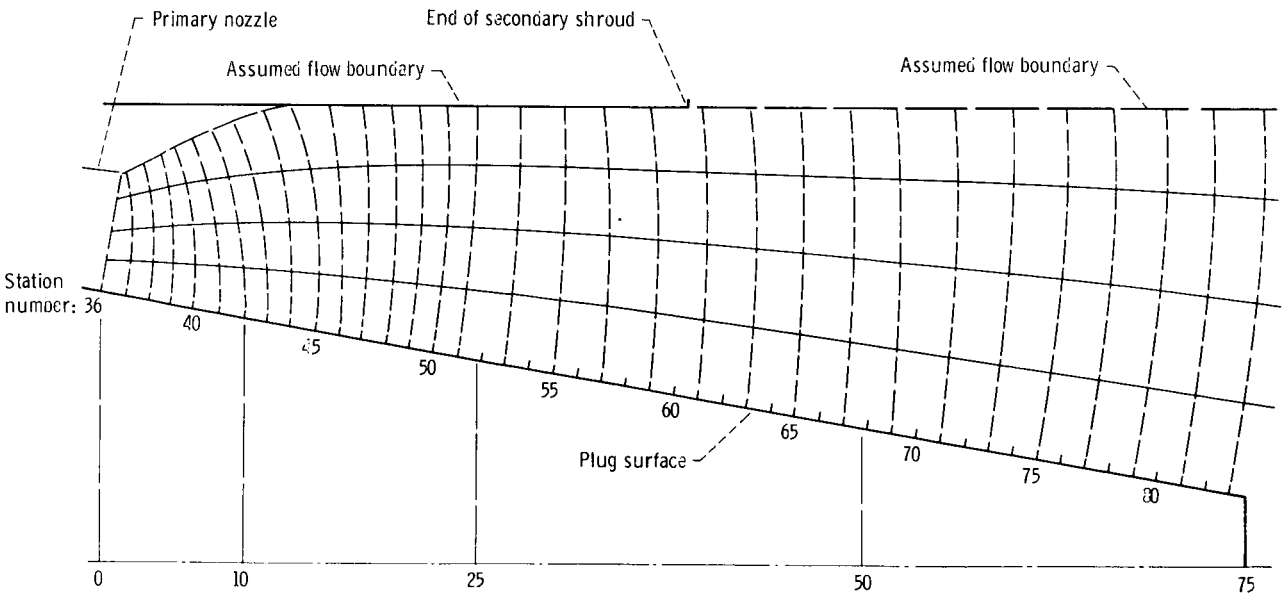

(b) Supersonic region.

Figure 21. - Equipotential lines used to calculate areas.

with the assumption that the primary flow remains attached to the plug:

$$R_{o,I} = \sqrt{\frac{A_8 \cos 10^o}{\left(\frac{A_8}{A}\right)_{max} \pi} + R_i^2} \tag{B6}$$

$$H' = \frac{R_o - R_i}{\cos 10^o} \tag{B7}$$

$$D_{h_{p,I}} = \frac{4A_8}{2\pi(R_i + R_o)\left(\frac{A_8}{A}\right)_{max}} \tag{B8}$$

The effective gas temperature was then calculated to account for high-speed flow effects.

$$T_{eff,I} = t_{p,I} + \Lambda(T_8 - t_{p,I}) \tag{B9}$$

where

$$\Lambda = \sqrt[3]{Pr_{ref}} \qquad \text{for turbulent flow} \tag{B10}$$

The reference Prandtl number was calculated as a function of reference temperature (ref. 17).

$$T_{ref,I} = 0.5\, T_{w,out,I} + 0.28\, t_{p,I} + 0.22\, T_{eff,I} \tag{B11}$$

Finally, a simple equation, originally developed for fully developed pipe flow, was included to calculate convective heat-transfer coefficients from the primary gas to the plug wall (ref. 10).

$$h_{p,I} = 0.026\,(Re_{ref})^{0.8}(Pr_{ref})^{0.3}\,\frac{k_{ref}}{D_{h_{p,I}}} \tag{B12}$$

Although this equation was believed to be reasonably accurate and was very easy to use, it was decided to compare the results from this equation with a more sophisticated boundary-layer procedure. Therefore, an option was included in the program to read in

values of local heat-transfer coefficient. Then, any of several existing boundary-layer programs could be used to calculate gas-to-wall heat transfer. The method selected for this study was developed by Bartz (ref. 11). The Bartz method solves the integral momentum and energy equations of the boundary layer in conjunction with a modified Von Karman momentum-heat analogy. The input to the Bartz program includes plug geometry and estimated wall temperature, total gas conditions, initial momentum boundary-layer thickness, and local Mach number. The problem that exists in using the Bartz program, as well as any other method of this type is the required local velocity or Mach number of the supersonic stream. As pointed out earlier, the estimate of local pressure (and, hence, velocity) is crude, at best, and may introduce more error than the difference between the Bartz coefficients and the pipe-flow coefficients.

The convective heat transfer from the gas to the wall is thus found:

$$q_{conv} = h_{p,I}(T_{eff,I} - T_{w,out,I}) \tag{B13}$$

Radiation. - Radiation from the hot combustion gases to the plug wall was calculated using a one-dimensional method described in reference 18.

$$q_{r,fl} = \frac{1}{2}\sigma(1 + a_w)\epsilon_{fl}t_{fl}^{1.5}\left(t_{fl}^{2.5} - T_{w,out,I}^{2.5}\right) \tag{B14}$$

The absorptivity of the wall a_w was assumed to be equal to 0.80 for this study. The flame emissivity was found from

$$\epsilon_{fl} = 1 - \exp\left[-18.5\ P_p\left(L_b\frac{f}{a}\right)^{1/2} T_{fl}^{-1.5}\right] \tag{B15}$$

This empirical correlation was developed for a nonluminous flame, and the model was said to be accurate when axial temperature gradients and end effects are small and the length-to-diameter ratio of the flame tube is large. The mean beam path length was defined to be

$$L_b = \frac{3.6\ (\text{Radiating volume})}{(\text{Receiving surface area})} \tag{B16}$$

For an axial increment ΔL this suggests that the mean beam path length is approximately equal to the local hydraulic diameter.

$$L_b = \frac{3.6\ (\text{Radiating volume})}{(\text{Receiving surface area})} \approx \frac{4\ (\text{Area})\ \Delta L}{(\text{Perimeter})\ \Delta L} = D_{h,I} \tag{B17}$$

Since the local hydraulic diameter varied considerably along the plug surface of the system studied and the mean beam path length is approximately equal to the hydraulic diameter, the local hydraulic diameter was taken to be the mean beam path length for this study. This is a good approximation along the sting support, where the flame radiation is highest. The flame radiation decreases considerably downstream, especially near the end of the supersonic plug surface.

Radiation from the sting support and the convectively cooled portion of the plug to the afterburner liner, the primary nozzle, the secondary shroud, and the atmosphere were neglected for this study. The afterburner liner (fig. 2) and iris primary would be approximately the same temperature as the sting support and plug surface; the net interchange of radiant energy should therefore be negligible. The translating secondary shroud will be retracted for acceleration to about Mach 1.2 and extended at higher Mach numbers. The temperature of the secondary shroud is a function of the amount of secondary air used, and this variable was not considered in this study. The net interchange should be from the plug to the secondary shroud, however. This is also the case for the radiation from the plug wall to the atmosphere. This term is only important near the end of the plug and, if included, would result in lower predicted plug wall temperatures in this region. Since the throat region was the critical convection-cooling region for the cases studied, the inclusion of this radiation term would not have altered the conclusions reached.

Wall temperature. - The heat entering the plug wall locally, then, was taken to be the sum of the convection from the hot combustion gases and radiation from the flame:

$$q = q_{conv} + q_{r,fl} \tag{B18}$$

The inner wall temperature $T_{w,i}$ (see fig. 6) was then calculated:

$$T_{w,i} = T_{w,out} - q\left(\frac{\tau_w}{k_w} + \frac{\tau_{fin}}{k_{fin}}\right) \tag{B19}$$

This equation assumes that the fin base occupies the entire space between fins. This is a reasonable assumption since, for the geometry selected, the distance between fins (Sp - W) is only about 20 percent greater than the fin width W on the average.

The coolant total temperature rise to the next station is, then,

$$\Delta T_c = \frac{qA}{\dot{w}C_p} \tag{B20}$$

Thus, the coolant total temperature at station $I + 1$ is calculated to be

$$T_{c,I+1} = T_{c,I} + \Delta T_c \tag{B21}$$

The heat flux loop (eqs. (B1) to (B21)) was repeated for each station from the coolant inlet to the end of the convective-cooling channel.

Coolant Pressure-Drop Loop

After completing the heat-flux calculations to obtain coolant temperatures, the coolant pressure calculations were performed from the discharge end of the passage, upstream, to the coolant inlet point. Choked flow is initially assumed at the end of the coolant channel. The total temperature, area, and flow rate are known. The static temperature was then found:

$$t = \frac{T}{\left[1 + \left(\frac{\gamma - 1}{2}\right)M^2\right]} \tag{B22}$$

And the total pressure was found from Fliegner's formula (ref. 19):

$$P = \frac{\dot{w}\sqrt{T_c}}{0.532\,AC_D} \tag{B23}$$

Nonisentropic flow was accounted for by including a discharge coefficient C_D of 0.98. Next, the static pressure at the choked flow station was calculated:

$$p = P\left[1 + \left(\frac{\gamma - 1}{2}\right)M^2\right]^{-\gamma/(\gamma-1)} \tag{B24}$$

This static pressure was then compared with the nozzle back pressure p_0. If the calculated static pressure was greater than p_0, the flow was, in fact, choked. If not, the flow was not choked, and the passage exit conditions were found by setting the static pressure equal to the back pressure and calculating the local static temperature and total pressure.

$$M = \frac{\frac{\dot{w}}{A} Rt_c}{p\sqrt{\gamma g Rt_c}} \tag{B25}$$

$$P = p\left[1 + \left(\frac{\gamma - 1}{2}\right)M^2\right]^{\gamma/(\gamma-1)} \tag{B26}$$

$$t_c = \frac{T_c}{\left[1 + \left(\frac{\gamma - 1}{2}\right)M^2\right]} \tag{B27}$$

The static temperature is initially set equal to the total temperature, and an iteration is required. Thus, the state of the fluid at the end of the convection-cooled channel is completely defined.

The following pressure-drop calculations were then made for each station from the passage exit upstream to the coolant inlet station. Average Reynolds number, specific flow rate, hydraulic diameter, and station length were found and friction factor calculated assuming turbulent flow in smooth tubes (ref. 14).

$$f = 0.0014 + \frac{0.125}{Re_{av}^{0.32}} \tag{B28}$$

Initially, the static pressure at station I is assumed to be equal to the static pressure at station I + 1. Then the static temperature at station I was calculated from the quadratic equation

$$\left[\left(\frac{\gamma - 1}{2}\right)\left(\frac{\dot{w}}{A}\right)_I^2 \frac{R}{p_I^2 \gamma g}\right] t_I^2 + t_I - T_I = 0 \tag{B29}$$

The static-pressure drop was found by summing the momentum and friction pressure drops:

$$\Delta p_m = \frac{\dot{w}^2}{A_{av} g}\left(\frac{1}{\rho_{I+1} A_{I+1}} - \frac{1}{\rho_I A_I}\right) \tag{B30}$$

$$\Delta p_{fr} = \frac{G_{av}^2}{g D_{h,av}} \left[\frac{4f \, \Delta L}{(\rho_I + \rho_{I+1})} \right] \tag{B31}$$

Thus,

$$p_I = p_{I+1} + \Delta p_m + \Delta p_{fr} \tag{B32}$$

An iteration was required until the calculated p_I was equal to the assumed p_I. On convergence, the Mach number and total pressure were calculated explicitly:

$$M_I = \frac{G_I}{\rho_I \sqrt{\gamma g R t_I}}$$

$$P_I = p_I \left[1 + \left(\frac{\gamma - 1}{2} \right) M^2 \right]^{\gamma/(\gamma-1)}$$

Expansion and contraction losses between fin sections were neglected as well as entrance losses at the turbine frame.

APPENDIX C

FILM-COOLING HEAT-TRANSFER ANALYSIS

The procedure used for predicting plug surface temperatures resulting from film cooling the aft end of the plug nozzle was based on the method of reference 8; it used the wall heat balance shown in figure 6(b). The internal plug temperature was assumed to be equal to the plug surface temperature. The axial conduction rate in the wall was assumed to be negligible. Also, the heat-transfer areas in the heat balance were assumed to be equal.

A heat balance on the wall (fig. 6(b)) was assumed wherein the hot-gas-to-wall radiation q_i was equal to the sum of the wall-to-coolant forced convection q_2 and the external-to-ambient radiation q_3

$$q_1 = q_2 + q_3 \tag{C1}$$

The hot-gas-to-wall radiation q_1 was calculated from the expression (ref. 14)

$$q_1 = \sigma\left(\frac{\epsilon_w + 1}{2}\right)\left(\epsilon_p t_{p,av}^4 - a_{gw} T_w^4\right) \tag{C2}$$

The wall-to-coolant forced convection q_2 was calculated from

$$q_2 = h_2(T_w - T_w') \tag{C3}$$

The external-to-ambient radiation q_3 was calculated from

$$q_3 = F_3\sigma\left(T_w^4 - t_{am}^4\right) \tag{C4}$$

By substituting the values for q_1, q_2, and q_3 as defined in equations (C2), (C3), and (C4), respectively, into equation (C1), an expression was obtained wherein all terms in the equation were determinable or expressed as a function of T_w. Equation (C1) was then solved using the Newton-Raphson method of iteration to determine the wall temperature assuming an initial estimate of the adiabatic wall temperature T_w' for T_w ($q_2 = 0$ for this assumption). The values used in equation (C2) to (C4) were determined as discussed in the next section.

Internal Flow Properties

The primary flow field was determined by assuming one-dimensional isentropic flow, hot-gas properties for the assumed ASTM A-1/air mixture, and uniform wall static pressure across the nozzle cross section. The wall static-pressure profile was assumed in accordance with the calculated pressure distribution line (figs. 7 and 16). The axial distance between the slot and the end of the plug was divided into equal increments. Local hot-gas flow properties at each station were determined and used in the heat balance (eqs. (C1) to (C4)) as required.

The coolant-flow field was determined by assuming that the air coming out of the plug convection-cooling passages flowed between the primary gas and the plug wall. To account for primary and coolant-stream thermal mixing, the local coolant properties were determined as follows. A semi-empirical film-cooling correlation was used to estimate a coolant-stream adiabatic wall temperature T'_w. This adiabatic wall temperature was assumed to represent the recovery temperature $T_{rec,c}$ of the coolant stream. Using the expression (ref. 20)

$$T_{rec,c} = t_c + Pr_c^{1/3} \frac{V_c^2}{2C_{p_c} gJ} \tag{C5}$$

together with the equation of state, continuity, and the air property tables, the local coolant-stream temperature t_c at each station was determined. Local coolant properties were determined at the local coolant temperature. The coolant-stream cross-sectional area was calculated by assuming isentropic flow from the coolant slot to match the wall static-pressure profile (figs. 7 and 16, calculated pressure distribution line).

All coolant-slot exit properties were calculated using isentropic equations, continuity, air property tables, the coolant-slot static temperature t_{sl}, the total coolant temperature T_c, and the total coolant pressure P_c, which was obtained from the convection-cooling analysis discussed in appendix B.

Hot-Gas-to-Wall Radiation

The primary gases were assumed to result from the combustion of ASTM A-1 (fuel) and air. Nonluminous radiation from the combustion products carbon dioxide and water vapor were considered and are accounted for in equation (C2). In order to solve equation (C2) (taken from ref. 14), values for $t_{p,av}$, ϵ_p, a_{gw}, and ϵ_w were required. The hot gas was assumed to radiate at each station at an average temperature $t_{p,av}$ which was obtained by averaging all local primary static temperatures from the slot to the end

of the plug. The values of emissivity ϵ_p and absorptivity a_{gw} for hot-gas radiation were estimated as outlined in reference 14 and as shown by equations (C6) and (C7):

$$\epsilon_p = \epsilon_{co} C_{co} + \epsilon_{wa} C_{wa} - \Delta\epsilon \tag{C6}$$

where

$$\epsilon_{co} = f(t_p, p'_{co} L_b)$$

$$\epsilon_{wa} = f(t_p, p'_{wa} L_b)$$

and where C_{co} is the correction for total-pressure effect for carbon dioxide, C_{wa} is the correction for total-pressure effect for water vapor, and $\Delta\epsilon$ is the correction for a mixture of CO_2 and H_2O. The absorptivity,

$$a_{gw} = a_{co} + a_{wa} - \Delta a \tag{C7}$$

where

$$a_{co} = f\left(T_w, p'_{co} L_b \frac{T_w}{t_p}\right)\left(\frac{t_p}{T_w}\right)^{0.65} C_{co}$$

$$a_{wa} = f\left(T_w, p'_{wa} L_b \frac{T_w}{t_p}\right)\left(\frac{t_p}{T_w}\right)^{0.45} C_{wa}$$

and where Δa is the correction for a mixture CO_2 and H_2O. Using an average hot-gas static temperature and static pressure at the stations being considered, the fuel-air ratio, and the method of reference 21, the mole fractional values for the products of combustion (for assumed equilibrium composition) were determined. The average hot-gas static pressure was multiplied by the mole fraction to obtain a partial pressure for the carbon dioxide p'_{co} and water vapor p'_{wa}. The mean beam length L_b was estimated with the use of the table 4-2 in reference 14. The hot gases were assumed to have a constant density and to form a concentric cylinder about the plug. The factor by which the characterizing dimension (ref. 14) is multiplied to obtain L_b was estimated by considering two radiating gas configurations: (1) a rectangular parallelepiped $1 : \infty : \infty$ (infinite parallel planes) running parallel to the plug surface radiating to a spot on the plug surface (fig. 22(b)) and, (2) an infinite cylinder of half circular cross section running along the plug surface and radiating to a spot on the plug surface (fig. 22(c)). It can be seen

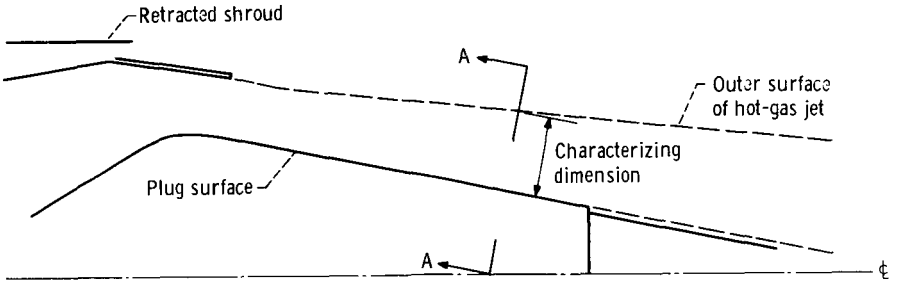

(a) Hot-gas jet geometry.

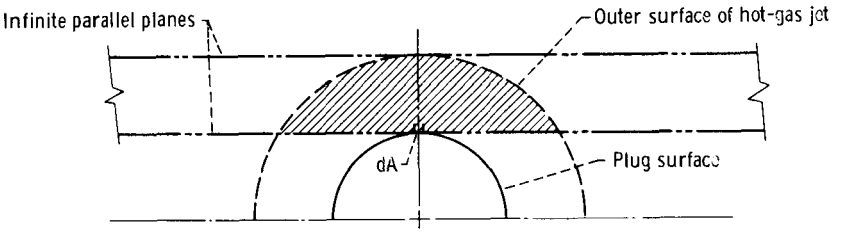

(b) Assumed hot-gas infinite parallel planes geometry (section A-A).

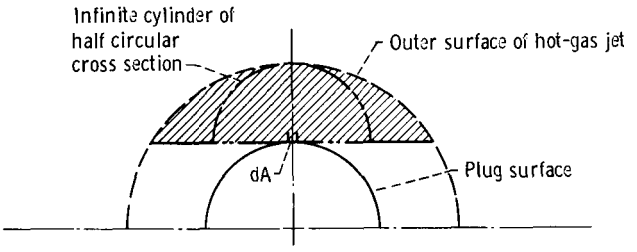

(c) Assumed hot-gas infinite cylinder of half cross section geometry (section A-A).

Figure 22. - Hot-gas configuration for determining mean beam length L_B.

that the actual hot-gas configuration is less than the infinite parallel plane configuration but greater than the infinite cylinder of half cross-section. The factor was therefore estimated accordingly to be 1.3.

The characterizing dimension was determined by finding the perpendicular distance from the plug surface to the outer surface of the hot-gas jet at a large number of stations along the plug and averaging these values. For the hot-gas jet configuration at takeoff conditions, the characterizing dimension was calculated to be 0.427 meter (1.4 ft). The mean beam length L_b then became 0.544 meter (1.82 ft). The partial pressure of the CO_2, or of the water vapor, whichever is applicable, was multiplied by the mean beam length to give $p'_{co}L_b$ or $p'_{wa}L_b$. Using these factors and the average hot-gas static temperature, ϵ_{co} and ϵ_{wa} at each station were determined from the charts of reference 14.

The total-pressure corrections C_{co} and C_{wa} were taken to be equal to 1.0 (ref. 22). The corrections for the interaction of CO_2 and H_2O ($\Delta\epsilon$) were about 10 percent and were omitted. Since the correction reduces the radiation, this omission makes the wall-temperature prediction more conservative. The emissivity of the gas ϵ_p then equals $\epsilon_{co} + \epsilon_{wa}$ (see eq. (C6)). Since an average hot-gas static temperature and average hot-gas partial pressure of CO_2 and H_2O were used, ϵ_p is the same for any plug cross section. On the other hand, a_{gw} is different at each station since it depends on T_w. Values of a_{co} and a_{wa} were obtained from charts (ref. 14) as functions of T_w and $p'_{co}L_b(T_w/t_p)$ or $p'_{wa}L_b(T_w/t_p)$. The values were corrected by multiplying by $(t_p/T_w)^{0.54}$ or $(t_p/T_w)^{0.45}$ as applicable (eq. (C7)) to obtain a_{co} and a_{wa}, respectively. Again, C_{co} and C_{wa} were assumed to equal to 1.0, and Δa was found to be about 4 percent and was neglected. In effect, this omission acts to increase the radiation and offset the effect of omitting $\Delta\epsilon$.

The plug surface was assumed to be gray. A factor, $(\epsilon_w + 1)/2$, to correct for this, was included in equation (C2), which was developed for black bodies. The wall emissivity ϵ_w was estimated to be 0.65 based on data in reference 23. The effect of increasing the emissivity ϵ_w to 0.9 was also investigated (see fig. 14).

Wall-to-Coolant Forced-Convection Heat-Transfer Rate (q_2)

The convective heat transfer at the wall (eq. (C3)) was based on the assumption that the potential for heat transfer was the difference between the wall temperature and the adiabatic wall temperature T'_w of the cooling film in a manner similar to that proposed in reference 24.

The adiabatic wall temperature T'_w at each station was determined with the use of the adiabatic wall film-cooling correlation proposed in reference 9 and modified to use an average value of the heat-transfer coefficient parameter $(\pi h D_{pl})_0^X$ from the point of

injection to the point of interest (as suggested in ref. 25). An experimental investigation on the application of the preceding correlation to the surface of a plug nozzle is reported in reference 6. The correlation is repeated here:

$$\ln\left(\frac{T_{rec,p} - T'_w}{T_{rec,p} - t_{sl}}\right) = -\left[\frac{\left(\pi h_f D_{pl}\right)_0^X}{\dot{w}_c C_{p,sl}} - 0.04\right]\left(\frac{SV_p}{\alpha_{sl}}\right)^{0.125} f\left(\frac{V_p}{V_{sl}}\right) \tag{C8}$$

where

$$h_f = 0.0265 \frac{k_f}{D_{pl}} Re_f^{0.8} Pr_f^{0.3} \tag{C9}$$

$$f\left(\frac{V_p}{V_{sl}}\right) = 1 + 0.4 \tan^{-1}\left(\frac{V_p}{V_{sl}} - 1\right) \qquad \text{for } \frac{V_p}{V_{sl}} \geq 1.0 \tag{C10}$$

For this study, V_p was always greater than V_{sl}.

The primary flow field properties were determined as indicated in the section on internal flow properties. The local hot-gas recovery temperature Tr_p was determined assuming turbulent flow (ref. 20):

$$Tr_p = t_p\left[1 + Pr_p^{1/3}\left(\frac{\gamma_p - 1}{2}\right)M_p^2\right] \tag{C11}$$

All coolant slot parameters (t_{sl}, $\dot{w}_s$, $C_{p,sl}$, α_{sl}, and V_{sl}) were evaluated at slot exit conditions.

A local heat-transfer coefficient $h_{f,X}$ (eq. (C9)) was determined using air fluid properties evaluated at a temperature t_f equal to an average of the local primary static temperature and the coolant slot inlet static temperature. The Reynolds number was based on

$$Re_f = \frac{\rho_f V_p D_{pl}}{\mu_f} \tag{C12}$$

where V_p is the local primary velocity.

The average value of the heat-transfer parameter $\left(\pi h_f D_{pl}\right)_0^X$ at a station was determined by multiplying π times the local values of $h_{f,X}$ and D_{pl} and then averaging this parameter with those calculated at all local stations from the slot to the station of interest.

The local heat-transfer coefficient h_2 was calculated using the standard flat-plate correlation for turbulent flow (ref. 20)

$$h_2 = 0.0296 \frac{k}{X} Re_X^{0.8} Pr^{1/3} \tag{C13}$$

where fluid properties were evaluated at an average of the adiabatic wall temperature T_w' and the wall temperature T_w. The coolant flow boundary layer was assumed to be turbulent and to originate at the coolant slot (fig. 6(b)). The local velocity, for the coolant stream Reynolds number, was determined as indicated in the section on internal flow properties.

Wall-to-Ambient Radiation (q_3)

The plug wall radiation is given by equation (C4) and depends on a configuration factor and t_{am}. The configuration factor F_3 was shown in reference 26 to equal ϵ_w for gray bodies. Here the constant values of $\epsilon_w = 0.65$ and 0.9 were assumed over the plug length. The ambient radiation temperature t_{am} was assumed to be 311 K (560° R).

REFERENCES

1. Beheim, Milton A.; Anderson, Bernhard H.; Clark, John S.; Corson, Blake W., Jr.; Stitt, Leonard E.; and Wilcox, Fred A.: Supersonic Exhaust Nozzles. Aircraft Propulsion. NASA SP-259, 1971, pp. 233-282.

2. Darchuk, George V.; and Balombin, Joseph R.: Noise Evaluation of Four Exhaust Nozzles for Afterburning Turbojet Engine. NASA TM X-2014, 1970.

3. Clark, John S.; Graber, Edwin J.; and Straight, David M.: Experimental Heat Transfer and Flow Results from an Air-Cooled Plug Nozzle System. NASA TM X-52897, 1970.

4. Huntley, S. C.; and Saminich, N. E.: Performance of a 10^{o} Conical Plug Nozzle Using a Turbojet Gas Generator. NASA TM X-52570, 1969.

5. Jeracki, Robert J.; and Chenoweth, Francis C.: Coolant Flow Effects on the Performance of a Conical Plug Nozzle at Mach Numbers from 0 to 2.0. NASA TM X-2076, 1970.

6. Chenoweth, Francis C.; and Lieberman, Arthur: Experimental Investigation of Heat-Transfer Characteristics of a Film-Cooled Plug Nozzle with Translating Shroud. NASA TN D-6160, 1971.

7. Bresnahan, Donald L.: Experimental Investigation of a 10^{o} Conical Turbojet Plug Nozzle with Iris Primary and Translating Shroud at Mach Numbers from 0 to 2.0. NASA TM X-1709, 1968.

8. Lieberman, Arthur: Comparison of Predicted and Experimental Wall Temperatures for a Cylindrical Ejector Exhaust Nozzle Operated with a Turbojet Gas Generator. NASA TN D-6465, 1971.

9. Hatch, James E.; and Papell, S. Stephen: Use of a Theoretical Flow Model to Correlate Data for Film Cooling or Heating an Adiabatic Wall by Tangential Injection of Gases as Different Fluid Properties. NASA TN D-130, 1959.

10. Bartz, D. R.: A Simple Equation for Rapid Estimation of Rocket Nozzle Convective Heat Transfer Coefficients. Jet Propulsion, vol. 27, no. 1, Jan. 1957, pp. 49-51.

11. Elliott, David G.; Bartz, Donald R.; and Silver, Sidney: Calculation of Turbulent Boundary-Layer Growth and Heat Transfer in Axi-Symmetric Nozzles. Tech. Rep. 32-387, Jet Propulsion Lab., California Inst. Tech., Feb. 15, 1963.

12. Freberg, Carl R.; and Kemler, E. N.: Elements of Mechanical Vibrations. Second ed., John Wiley & Sons, Inc., 1949.

13. Poferl, David J.; Svehla, Roger A.; and Lewandowski, Kenneth: Thermodynamic and Transport Properties of Air and the Combustion Products of Natural Gas and of ASTM A-1 Fuel with Air. NASA TN D-5452, 1969.

14. McAdams, William H.: Heat Transmission. Third ed., McGraw-Hill Book Co., Inc., 1954.

15. Schneider, Paul J.: Conduction Heat Transfer. Addison-Wesley Publ. Co., 1955.

16. Zucrow, Maurice J.: Aircraft and Missile Propulsion. Vol. I. John Wiley & Sons, Inc., 1958.

17. Eckert, Ernst R. G.; and Drake, Robert M., Jr.: Heat and Mass Transfer. Second ed., McGraw-Hill Book Co., Inc., 1959.

18. Anon.: Computer Program for the Analysis of Annular Combustors. Vol. I: Calculation Procedures. Rep. 1111-1, vol. 1, Northern Research and Engineering Corp. (NASA CR-72374), Jan. 29, 1968.

19. Shapiro, Ascher H.: The Dynamics and Thermodynamics of Compressible Fluid Flow. Vol. I. Ronald Press Co., 1953.

20. Rohsenow, Warren M.; and Choi, Harry: Heat, Mass, and Momentum Transfer. Prentice-Hall, Inc., 1961.

21. Zeleznik, Frank J.; and Gordon, Sanford: A General IBM 704 or 7090 Computer Program for Computation of Chemical Equilibrium Compositions, Rocket Performance, and Chapman-Jouguet Detonations. NASA TN D-1454, 1962.

22. Hottel, H. C.; and Egbert, R. B.: Radiant Heat Transmission from Water Vapor. Trans. AIChE, vol. 38, no. 3, June 25, 1942, pp. 531-565.

23. Wolf, J., ed.: Aerospace Structural Metals Handbook. Vol. IIA. Non-Ferrous Alloys. Belfour Stulen, Inc. (AFML-TR-68-115), 1968.

24. Hartnett, J. P.; Birkebak, Richard C.; and Eckert, E. R. G.: Velocity Distributions, Temperature Distributions, Effectiveness, and Heat Transfer for Air Injected Through a Tangential Slot into a Turbulent Boundary Layer. Paper 60-HT-31, ASME, 1960.

25. Lucas, James G.; and Golladay, Richard L.: Gaseous-Film Cooling of a Rocket Motor with Injection Near the Throat. NASA TN D-3836, 1967.

26. Chenoweth, Francis C.; and Steffen, Fred W.: Comparison of Experimental and Predicted Heat-Transfer Characteristics for a Cylindrical Ejector. NASA TM X-1641, 1968.

1. Report No.	2. Government Accession No.	3. Recipient's Catalog No.
NASA TM X-2475		

4. Title and Subtitle	5. Report Date
THERMAL DESIGN STUDY OF AN AIR-COOLED PLUG-NOZZLE SYSTEM FOR A SUPERSONIC-CRUISE AIRCRAFT	January 1972
	6. Performing Organization Code

7. Author(s)	8. Performing Organization Report No.
John S. Clark and Arthur Lieberman	E-6348
	10. Work Unit No. 764-74

9. Performing Organization Name and Address	11. Contract or Grant No.
Lewis Research Center National Aeronautics and Space Administration Cleveland, Ohio 44135	

12. Sponsoring Agency Name and Address	13. Type of Report and Period Covered
National Aeronautics and Space Administration Washington, D.C. 20546	Technical Memorandum
	14. Sponsoring Agency Code

15. Supplementary Notes

16. Abstract

A heat-transfer design analysis has been made of an air-cooled plug-nozzle system for a supersonic-cruise aircraft engine. The proposed 10^{o} half-angle conical plug is sting supported from the turbine frame. Plug cooling is accomplished by convection and film cooling. The flight profile studied includes maximum afterburning from takeoff to Mach 2.7 and supersonic cruise at Mach 2.7 with a low afterburner setting. The calculations indicate that, for maximum afterburning, about 2 percent of the engine primary flow, removed after the second stage of the nine-stage compressor, will adequately cool the plug and sting support. Ram air may be used for cooling during supersonic-cruise operation, however. Therefore, the cycle efficiency penalty paid for air cooling the plug and sting support should be low.

17. Key Words (Suggested by Author(s))	18. Distribution Statement
Plug nozzle, Heat transfer, Cooling, Film cooling, Supersonic, Turbojet, Afterburning convection design	Unclassified - unlimited

19. Security Classif. (of this report)	20. Security Classif. (of this page)	21. No. of Pages	22. Price*
Unclassified	Unclassified	50	$3.00

* For sale by the National Technical Information Service, Springfield, Virginia 22151